NASA MEMO 1-18-59A

NASA

MEMORANDUM

SUBSONIC WING LOADINGS ON A 45° SWEPTBACK-WING AND BODY COMBINATION AT HIGH ANGLES OF ATTACK

By John A. Axelson and Jack F. Haacker

Ames Research Center
Moffett Field, Calif.

NATIONAL AERONAUTICS AND SPACE ADMINISTRATION
WASHINGTON
February 1959

NATIONAL AERONAUTICS AND SPACE ADMINISTRATION

MEMORANDUM 1-18-59A

SUBSONIC WING LOADINGS ON A 45° SWEPTBACK-WING AND BODY COMBINATION AT HIGH ANGLES OF ATTACK

By John A. Axelson and Jack F. Haacker

SUMMARY

A study has been made of the subsonic pressure distributions and loadings for a 45° sweptback-wing and body combination at angles of attack up to 36°. The wing had an aspect ratio of 5.5, a taper ratio of 0.53, and NACA 64A010 sections normal to the quarter-chord line and was mounted on a slender body of fineness ratio 12.5. Test results are presented for Mach numbers of 0.30 and 0.50 with corresponding Reynolds numbers of 1.5 and 2.0 million, respectively.

The stall patterns and spanwise loadings at high angles of attack for the present model are correlated with those for other 45° sweptback-wing and body combinations having aspect ratios between 4.0 and 8.0. A tentative approach is presented for extrapolating the Weissinger span-loading method to higher angles of attack, and for deriving the spanwise-load distributions for 45° sweptback wings at angles of attack above 20°.

The investigation also included tests of the body in combination with only one panel of the swept wing. The problem of estimating the normal-force coefficient for the single panel at high angles of attack is considered.

INTRODUCTION

Swept-wing aircraft frequently exceed angles of attack of 20° during inadvertent maneuvers such as result from pitch-up or inertia cross coupling. No methods are available for predicting the loadings at these high angles, and relatively little is understood concerning the complex flow fields which develop around the wing as discussed in references 1 and 2. To meet the problems which arise at high angles of attack, both the researcher and the aircraft designer must rely heavily on the relatively small amount of available experimental data.

The purposes of the present report are to present some additional experimental loadings at high angles of attack and to attempt a correlation and analysis of the results. A study is made of the pressure distributions, normal-force coefficients, and centers of pressure for the model with the complete swept wing and with one wing panel only. The

experimental results are correlated with those for other 45° sweptback-wing and body combinations from references 3 and 4 and from unpublished data. A tentative approach is presented for estimating sweptback-wing loadings at high angles of attack. The study is restricted to sweptback wings having sweep angles of approximately 45° and aspect ratios between 4.0 and 8.0. Exact expressions for velocity components and for component angles of attack are presented (appendix A) to replace the heretofore used linearized relations of simple sweep theory which are valid only at small angles of attack. The effects of Mach number are not considered.

NOTATION

A aspect ratio of sweptback wing, $\frac{b^2}{S}$

A_r reduced aspect ratio of one panel of a sweptback wing as approximated by a rectangular surface (fig. 24(a))

b wing span

b' span of the low-aspect-ratio wing (fig. 24(a))

C_L lift coefficient, $\frac{\text{lift}}{qS}$

C_m pitching-moment coefficient about the lateral axis through $\frac{\bar{c}}{4}$;

from force data for the wing-body combination, $\frac{\text{pitching moment}}{qS\bar{c}}$;

from pressure data for the wing panel,

$$\int_o^1 \left(c_m \frac{c^2}{\bar{c} c_{av}} + c_n \frac{cd}{\bar{c} c_{av}} \right) d\eta$$

c_m section pitching-moment coefficient about the lateral axis through $\frac{c}{4}$, $\int_o^1 \Delta C_p \frac{(c/4 - x)}{c} d\frac{x}{c}$

C_N normal-force coefficient:

from force data, $\frac{\text{normal force}}{qS}$;

from pressure data, $\int_o^1 c_n \frac{c}{c_{av}} d\eta$

C_N' normal-force coefficient of an unyawed, low-aspect-ratio wing

c_n section normal-force coefficient, $\int_0^1 \Delta C_p d\frac{x}{c}$

C_p pressure coefficient, $\frac{p - p_\infty}{q}$

ΔC_p lower surface pressure coefficient minus upper surface pressure coefficient

c local wing chord

c_{av} average wing chord

c_r root chord

c_t tip chord

$\bar{c}$ wing mean aerodynamic chord, $\frac{\int_0^1 c^2 d\eta}{\int_0^1 c d\eta}$

d longitudinal distance between the lateral axes through $\frac{\bar{c}}{4}$ and through $\frac{c}{4}$, positive when forward of $\frac{\bar{c}}{4}$

M Mach number

p local static pressure

p_∞ free-stream static pressure

q free-stream dynamic pressure

S wing area

V velocity

x longitudinal distance

y lateral distance

α angle of attack of wing plane

η dimensionless lateral coordinate, $\frac{2y}{b}$, measured from center line along the quarter-chord line

η' dimensionless lateral coordinate measured from mid-semispan (fig. 17)

η^* dimensionless length of bound leading-edge vortex on single panel (fig. 24)

Λ average angle of sweep of the wing

λ taper ratio

Subscripts

b velocity components or angles in a plane perpendicular to the plane of the wing and passing through the midchord line of the swept-wing panel or through the midspan of the equivalent wing of reduced aspect ratio

n velocity components or angles in planes perpendicular to the wing plane and the midchord line

∞ free stream

APPARATUS AND MODEL

The investigation was conducted in the Ames 14-foot transonic wind tunnel, which is a closed-circuit, return-type tunnel having a flexible-wall nozzle and a perforated test section and operating at atmospheric total pressure. The model was mounted on the sting-support system shown in figure 1. The model studied in reference 5 was used for the present investigation and is shown in figure 2. The swept wing was symmetrically mounted on the center line of the fuselage, which was a Sears-Haack body having a theoretical fineness ratio of 12.50 but cut off at 81 percent of closure to facilitate sting mounting. The wing had an aspect ratio of 5.50, a taper ratio of 0.53, and NACA 64A010 airfoil sections in planes perpendicular to their own quarter-chord line which was swept back 45°.

TESTS AND CORRECTIONS

Tests

The wind-tunnel program included tests at angles of attack from 0° to 36° in 4° increments for Mach numbers of 0.30 and 0.50 with corresponding Reynolds numbers of 1.5 million and 2.0 million based on the mean aerodynamic chord. Forces and moments were measured for the body alone and for the body with the complete wing by means of an electrical strain-gage balance housed within the model. Pressure distributions were measured on the upper and lower surfaces of the wing at five

stations, as shown in figure 2, for the body with the complete wing and with one wing panel only. Records of the pressures were obtained by photographing multiple-tube, mercury-filled manometers connected to the model orifices. The percent-chord locations of the orifices comprising the inboard and tip stations are measured in the streamwise direction, while those for the three intermediate stations are along chords perpendicular to the quarter-chord line as shown in figure 2. The streamwise orientation of the root and tip orifices slightly changes the airfoil section, the pressure distributions, and the integrated characteristics at these stations. These effects are considered small enough to be neglected in the present study.

Corrections

No corrections for wall-interference effects are deemed necessary because the model blockage was less than 0.06 percent, and because of the porous-wall test section in which the tests were conducted. No base pressure corrections were applied because the model base pressures were sufficiently close to free-stream static pressure to render the corrections negligible.

Precision

The accuracy of the results based on the sensitivity of the measuring apparatus and the repeatability of the data is considered to be within the following limits:

C_p	±0.03
C_L, C_N, c_n	±0.01
C_m	±0.005
M	±0.005
α	±0.1°

RESULTS

Presentation of Experimental Data and Results

Pressure distributions.- The chordwise pressure distributions for each of the five wing stations are shown in figures 3 through 7. Selected pressure distributions and wing upper surface isobars, such as were shown in reference 5, at lower angles of attack are presented in figure 8 for a Mach number of 0.50. All experimental pressure data presented include results for both the model with the complete wing and with one wing panel only.

Section normal-force coefficients and centers of pressure.- The variations with angle of attack of the section normal-force coefficients and of the chordwise locations of the centers of pressure for each of the five wing stations are presented in figures 9 and 10, respectively. The spanwise variations of section normal-force coefficient at each angle of attack are shown in figure 11. While the distributions in figure 11 are not actually loading curves, they will be discussed as such, since they differ from loading curves only by the ratio of local chord to average chord. The spanwise locations of the centroids of the weighted span loadings, $c_n c/c_{av}$, are shown in figure 12.

Integrated pressure data and force data.- The variations with angles of attack of the integrated wing normal-force coefficients and wing pitching-moment coefficients for the one- and two-wing-panel model configurations are shown in figures 13 and 14, respectively. The integrations covered the areas enclosed within the curves of figure 11 extrapolated to the body center line. Included in figures 13 and 14 are the corresponding coefficients for the model with the complete wing obtained from the force tests. Figure 15 presents the lift- and normal-force coefficients from the force tests for the body alone and for the body with the complete wing.

DISCUSSION

Measured Characteristics of the Complete Sweptback Wing

Pressure distributions.- As shown in figures 3 through 8, there was relatively little difference between the lower surface pressure distributions for each of the five wing stations for any given angle of attack. The maximum calculated pressure coefficient at zero angle of attack for a leading edge swept back 46.7° is 0.47, based on recovery of the dynamic pressure normal to the leading edge. The experimental values increased to as high as 0.70 at 36° angle of attack (fig. 3(i)), partly because the resultant sweep angle effectively decreased with increasing angle of attack. (At an angle of attack of 90°, the wing lower surface would be unswept relative to the air stream and would develop the full stagnation pressure over a limited region such as occurs with a plate normal to the air stream.)

In contrast to the lower surface pressure distributions, those for the upper surface exhibited some significant differences between the inboard and outboard portions of the wing in the range from above about 10° to 20° angle of attack. As shown in figure 8(a), there were negative-pressure-coefficient peaks near the leading edge at all stations at 8°. As the angle of attack was increased to 16°, the peaks disappeared from the outboard pressure distributions while becoming more pronounced in the inboard pressure distributions at $\eta = 0.2$. Above 20° the upper

surface pressure distributions for all stations were essentially flat, but the pressure coefficients for the outboard stations continued to become more negative with further increase in angle of attack.

Section characteristics.- As had been noted in references 5 and 6 for angles of attack below 20°, the inboard wing stations developed considerably higher loadings than did the outboard stations. The maximum measured section normal-force coefficient for the swept wing was 1.5 (fig. 9(a)). Each curve of section normal-force coefficient versus angle of attack exhibited an initial peak, the peaks occurring at higher angles of attack the more inboard the station. (The results of reference 5 were measured for smaller increments of angle of attack and were used as a guide in the fairing of figure 9.) Above the angles of attack for the initial peaks, the section centers of pressure tended to converge to 40-percent chord as shown in figure 10.

Integrated wing characteristics.- The spanwise distributions of section normal-force coefficient (fig. 11) were relatively flat at the lowest angles, decidedly steep and inwardly concentrated at 20°, then progressively flattened again with further increase in angle of attack. The centroids of the actual loadings (weighted for local chord) shown in figure 12 indicate an inboard and consequently forward shift for angles of attack up to 20°. These shifts in the location of the centroids are reflected in the pitching-moment characteristics presented in figure 14.

Force data.- Comparison of the integrated pressure results and the force data for the complete wing and body shows that the body produced a sizable effect on the pitching-moment coefficients (fig. 14), indicating a large lever arm to the body center of pressure which was probably near the leading edge of the wing root chord. The lift and normal-force coefficients for the body alone were less than 10 percent of those for the complete wing-body combination (fig. 15). The detailed study of the effects of the body on the loading of a 45° sweptback-wing and body combination, presented in reference 3, concluded that the body lift was nearly the same as the lift carried by the same area on the wing without the body, that is, the wing area blanketed by the body. The distribution of the loading on the wing, however, may be affected by the body interference, and application of the method of reference 3 to the wing of the present model indicated a maximum change in section normal-force coefficient of 20 percent at the inboard station. The effect of the body on the wing section loadings converges to zero with increasing distance along the span (see figs. 8 and 9 of ref. 3). There was close agreement between the over-all normal-force coefficients derived from integration of the wing pressures and those measured for the wing and body with the force balance (fig. 13).

Correlation of Sweptback Wings

Section normal-force characteristics.- In order to seek some order to the seemingly complex behavior of the swept wing at high angles of attack, the results of the present test were compared with those from other studies of 45° sweptback-wing and body combinations listed in table I. To simplify the comparison, wings with camber, twist, fences, flaps, chord extensions, and aspect ratios below 4.0 were not included. As shown in figure 16(a), a degree of correlation existed between the angles of attack at which the first peak or maximum occurred in the section normal-force coefficients, that is, where $dc_n/d\alpha \approx 0$. The section normal-force coefficients corresponding to the peaks and shown in figure 16(b) were not so invariant but rather appeared to vary with Reynolds number. (The values for the present test were approximately the same at both Mach numbers, and the averages are shown in figure 16.)

At angles of attack of 20° and 24°, the highest angles common to all of the tests, the spanwise variations of section normal-force coefficient were compared as shown in figure 17. The correlation was again fairly close in view of the many differences in model geometry and test conditions (table I). It should not be concluded that variables, such as Reynolds number, taper ratio, and airfoil section, have no effect at high angles of attack, but it does appear that for the range of plan forms considered, such effects were relatively small.

Spanwise distribution of c_n.- The average of the five sets of data for an angle of attack of 20° (fig. 17(a)) was approximated by the superposed distribution function often used for convenience in mathematical studies such as in references 7, 8, and 9. Because this function extends to infinity, it is not an accurate representation of actual loadings. Suitably modified for higher angles of attack, as shown in figure 18, the new function, containing no singularity, conforms with the flattening of the c_n distributions above 20° as shown in figure 19. (The continued flattening of the function above 36° lacks experimental verification at the present.)

Estimated Section Loads for the Sweptback Wing

The observations made while attempting to establish some order to the collection of swept-wing results at high angles of attack can perhaps be best organized by considering a tentative method for estimation of the section normal-force coefficients for the present swept-wing model (fig. 20). Below 10°, accurate estimates are possible with the Weissinger method summarized in reference 10. Between 10° and 20°, the correlated angles of attack from figure 16(a) provide useful limits for the extrapolation of the Weissinger estimates. Above 20°, the total normal-force coefficients from force data, if available, may be tentatively distributed

according to the distribution function of figure 18. If the total normal-force coefficients were not available, the absence of any method for their estimation would lead to an impasse. With no pretense at rigor, the single-panel estimate of appendix B distributed according to figure 18 has also been included in the figure to indicate the estimate obtained when total normal force is not known.

CONCLUDING REMARKS

A study has been made of the subsonic aerodynamic loading characteristics of a 45° sweptback-wing and body combination at high angles of attack, where no previous systematic correlation or suitable theory has been available. A degree of correlation was found between the stall patterns and spanwise-load distributions for the present model and for three other 45° sweptback-wing and body combinations having plain wings of aspect ratios from 4.0 to 8.0. The correlation was considered useful for extrapolating the Weissinger span-loading method to higher angles of attack for wings similar to those included in the correlation. A tentative approach has been introduced wherein the normal forces on a sweptback wing can be distributed across the span for angles of attack above 20°. A study of the measured loadings on a single panel of the swept wing and a tentative method for approximating the normal-force coefficient have been included in the appendix.

It appears that a further understanding of swept-wing loadings at high angles of attack can best be gained by fundamental research into the behavior of vorticity and separation on swept edges, both sharp and rounded, including the assessment of the effects of Reynolds number and Mach number.

Ames Research Center
National Aeronautics and Space Administration
Moffett Field, Calif., Oct. 22, 1958

APPENDIX A

EXACT RELATIONS FOR VELOCITY AND ANGLE-OF-ATTACK COMPONENTS

At the high angles of attack being considered in the present study, account must be taken of the inclination of the plane of the sweptback wing to the free-stream velocity. The resolution of the free-stream velocity into two mutually perpendicular velocity components both of which lie in the horizontal plane is no longer adequate. The resolution can be accomplished with useful results, however, if one of the two velocity components is kept in the inclined plane of the wing. The two velocity components may be designated as the normal velocity component V_n which lies in a plane containing a chord normal to the midchord line of the swept wing, and the spanwise velocity component V_b which lies in a plane directed along a constant percent-chord line (usually the midchord line). Both of these mutually perpendicular velocity components lie in the plane of the wing only at zero angle of attack. At all other angles of attack, only one of the components can be kept in the wing plane, while the other will meet the wing at an angle of attack α_n or α_b, the subscript matching the velocity component in question.

Case 1: $\alpha_b = 0$

If the spanwise velocity component V_l is kept in the plane of the wing and directed along a line of constant percent chord, the following exact relations apply:

$$\left.\begin{aligned} \alpha_b &= 0 \\ \alpha_n &= \sin^{-1}\left(\frac{\sin\alpha}{\cos\Lambda\sqrt{1 + \tan^2\Lambda \sin^2\alpha}}\right) \\ V_b &= V_\infty \sin\Lambda \cos\alpha \\ V_n &= V_\infty \cos\Lambda \sqrt{1 + \tan^2\Lambda \sin^2\alpha} \end{aligned}\right\} \qquad \text{(A1)}$$

Case 2: $\alpha_n = 0$

If the normal velocity component V_n is kept in the plane of the wing and directed along a normal chord, the following relations hold:

$$\left.\begin{aligned} \alpha_n &= 0 \\ \alpha_b &= \sin^{-1}\left(\frac{\sin\alpha}{\sin\Lambda\sqrt{1+\cot^2\Lambda\sin^2\alpha}}\right) \\ V_n &= V_\infty \cos\Lambda\cos\alpha \\ V_b &= V_\infty \sin\Lambda\sqrt{1+\cot^2\Lambda\sin^2\alpha} \end{aligned}\right\} \qquad \text{(A2)}$$

The velocity ratio V_b/V_∞ and the angle-of-attack component α_b for case 2 are plotted in figure 21. Only case 2 is required for the analysis presented in appendix B.

APPENDIX B

CHARACTERISTICS OF THE SINGLE PANEL

Comparison of Experimental Results for the Single Panel and the Complete Wing

In an attempt at furthering the understanding of loads on sweptback wings at high angles of attack, the present study included the measurement of the experimental pressure distributions for the model with one wing panel removed. Some marked differences in the section characteristics for the inboard stations and some equally interesting similarities in the over-all normal forces for the single-panel and complete-wing model configurations bear noting.

Pressure distributions.- There were no noteworthy differences between the lower surface pressure distributions for the single panel and complete wing, but the upper surface distributions for the inboard stations differed significantly, especially above 20° (figs. 3(f) to 3(i)). Prominent negative-pressure-coefficient peaks disappeared from the distributions for the complete wing above 20°, but persisted in the distributions for the single panels to 36°.

Section characteristics.- The aforementioned peaks in the inboard upper surface pressure distributions for the single panel at the high angles of attack were generally reflected in the correspondingly higher section normal-force coefficients in figures 9 and 11. The resulting change in the angles of attack at which the initial peaks occurred in the section normal-force coefficients (fig. 9) is shown in figure 22. The similarities in the pressure distributions at the higher angles of attack for all but the inboard station resulted in a general convergence (fig. 10) of the section centers of pressure to approximately 40-percent chord.

Normal-force coefficient.- The integrated normal-force coefficients for the single panel were less than those for the complete wing at angles of attack below 24°, but were higher at 36° by 10 percent at 0.3 Mach number and by 25 percent at 0.5 Mach number (fig. 13). Above 20°, at both Mach numbers, the integrated normal-force coefficients for the single panel were within 15 percent of those for the complete-wing model determined from the force measurements. At both Mach numbers and for all angles of attack, the centroids of the actual loadings on the single panel and on the complete wing were within 4-percent wing semispan as shown in figure 12.

Estimated Single-Panel Normal-Force Coefficient

It is interesting to direct attention to the problem of estimating the over-all normal-force coefficients on the single panel of the swept wing (fig. 23). An empirical approach follows which considers the single panel as a yawed, low-aspect-ratio wing, uses the exact relations for the components of velocity and angles of attack from appendix A, and uses the single-panel experimental results (fig. 22) as a guide in the assumption of a suitable, simplified, conceptual vortex model.

Vortex model.- The single panel will be assumed to be represented by an equivalent surface of low aspect ratio indicated by the dashed lines in figure 24(a). A single horseshoe-type vortex such as used in reference 11 for the unyawed wing will be assumed to represent the equivalent low-aspect-ratio surface as shown in figure 24(b). To account for the effect of sweep, which may be considered to be the complement of the yaw angle, the velocity is resolved into the components shown in figure 24(c). The vortex is assumed to have a segment of length η^* which would produce no lift in unyawed attitude but which now may be considered bound with respect to the normal velocity component V_n. The initial abrupt changes in the section normal-force coefficients (fig. 9) were assumed to be indicative of the shedding of vorticity at the angles of attack shown in figure 22. Because the pressure-distribution stations were identified by their spanwise intersections with the panel quarter-chord line, η^* was determined outboard of the intersection of the latter line with b', namely, outboard of $\eta = 0.3$ as shown in figure 22.

Normal-force coefficient.- The normal-force coefficients for the yawed wing of low aspect ratio ($A_r = 0.22$) may be expressed as the sum of the contributions of each of the two bound segments of the vortex. The first contribution, designated $C_N'(V_b/V_\infty)^2$, results from the segment along b' whose normal velocity is V_b. The normal-force coefficient C_N' was determined from the unyawed data in references 12 and 13 for the angle of attack α_b. The contribution of the second segment may be related to that of the first by the Kutta-Joukowsky law. If the contributions are proportional to the lengths of the segments and to the respective normal velocity components, the normal-force coefficient may be expressed as

$$C_N = C_N'\left(\frac{V_b}{V_\infty}\right)^2\left(1 + \frac{V_n\eta^* b/2}{V_b b' \cos\Lambda}\right)$$

$$= C_N'\left(\frac{V_b}{V_\infty}\right)^2\left(1 + \frac{V_n\eta^*}{V_b A_r}\right) \qquad \text{(B1)}$$

The normal-force coefficients estimated from equation (B1) in which η^* is derived from figure 22 are compared with those measured experimentally for the single panel in figure 23. (If the same degree of correlation exists for single panels as existed for the complete wings in figure 16(a), then the values of η^* in figure 22 might apply for other 45° sweptback panels whose plan forms approximated that of the present model.)

REFERENCES

1. Kirby, D. A., and Spence, A.: Low-Speed-Tunnel Model Tests on the Flow Structure Behind a Delta-Wing Aircraft and a 40 deg Swept-Wing Aircraft at High Incidences. R. and M. 3078, 1958. (Also available as R.A.E. TN Aero. 2361, April 1955)

2. Elle, B. J.: A Note on the Vorticity Distribution on the Surface and in the Wake of Slender Delta Wings with Leading Edge Separation. A.R.C. 19,779, Jan. 1958. (Also available as A.R.C. F.M. 2628, and Perf. 1620)

3. Martina, Albert P.: The Interference Effects of a Body on the Spanwise Load Distributions of Two 45° Sweptback Wings of Aspect Ratio 8.02 from Low-Speed Tests. NACA TN 3730, 1956. (Supersedes NACA RM L51K23)

4. Silvers, H. Norman, King, Thomas J., Jr., and Alford, William J., Jr.: Wind-Tunnel Investigation at High Subsonic Speeds of the Effects of Wing-Mounted External Stores on the Loading and Aerodynamic Characteristics in Pitch of a 45° Sweptback Wing Combined With a Fuselage. NACA RM L54A21, 1954.

5. Walker, Harold J., and Maillard, William C.: A Correlation of Airfoil Section Data With the Aerodynamic Loads Measured on a 45° Sweptback Wing Model at Subsonic Mach Numbers. NACA RM A55C08, 1955.

6. Hunton, Lynn W.: Effects of Finite Span on the Section Characteristics of Two 45° Sweptback Wings of Aspect Ratio 6. NACA TN 3008, 1953. (Supersedes NACA RM A52A10)

7. Von Kármán, Th., and Burgers, J. M.: General Aerodynamic Theory - Perfect Fluids. Theory of Airplane Wings of Infinite Span. Vol. II of Aerodynamic Theory, div. E, ch. III, sec. 7, W. F. Durand, ed., C.I.T., Pasadena, 1943, pp. 37-39.

8. Betz, A.: Applied Airfoil Theory. Properties of Typical Profiles. Vol. IV of Aerodynamic Theory, div. J, ch. II, sec. 1, W. F. Durand, ed., C.I.T., Pasadena, 1943, pp. 26-29.

9. Bollay, W.: A Nonlinear Wing Theory and Its Application to Rectangular Wings of Small Aspect Ratio. Z.a.M.M., vol. 19, no. 1, Feb. 1939, pp. 21-35.

10. DeYoung, John, and Harper, Charles W.: Theoretical Symmetric Span Loading at Subsonic Speeds for Wings Having Arbitrary Plan Form. NACA Rep. 921, 1948.

11. Weinig, F.: Lift and Drag of Wings with Small Span. NACA TM 1151, 1947.

12. Winter, H.: Flow Phenomena on Plates and Airfoils of Short Span. NACA TM 798, 1936.

13. Michael, William H., Jr.: Flow Studies in the Vicinity of a Modified Flat-Plate Rectangular Wing of Aspect Ratio 0.25. NACA TN 2790, 1952.

TABLE I.- MODEL DETAILS AND TEST CONDITIONS FOR THE CORRELATION OF EXPERIMENTAL LOADINGS ON 45° SWEPTBACK-WING AND BODY COMBINATIONS IN FIGURES 16 AND 17

A	λ	NACA section	Wind tunnel	Reynolds number, million	Mach number	α_{max}, deg	Reference
4.0	0.60	65A006s	Langley 7 by 10	2.1	0.50	24	RM L54A21
5.5	.53	64A010	Ames 14-foot	1.5,2.0	0.30,0.50	36	Present test and RM A55C08
6.0	.29	64A010	Ames 40 by 80	8.0	0.19	24	Unpublished
8.0	.45	63A012s	Langley 19-foot	4.0	0.19	29	TN 3730

s denotes streamwise; others normal to c/4 line.

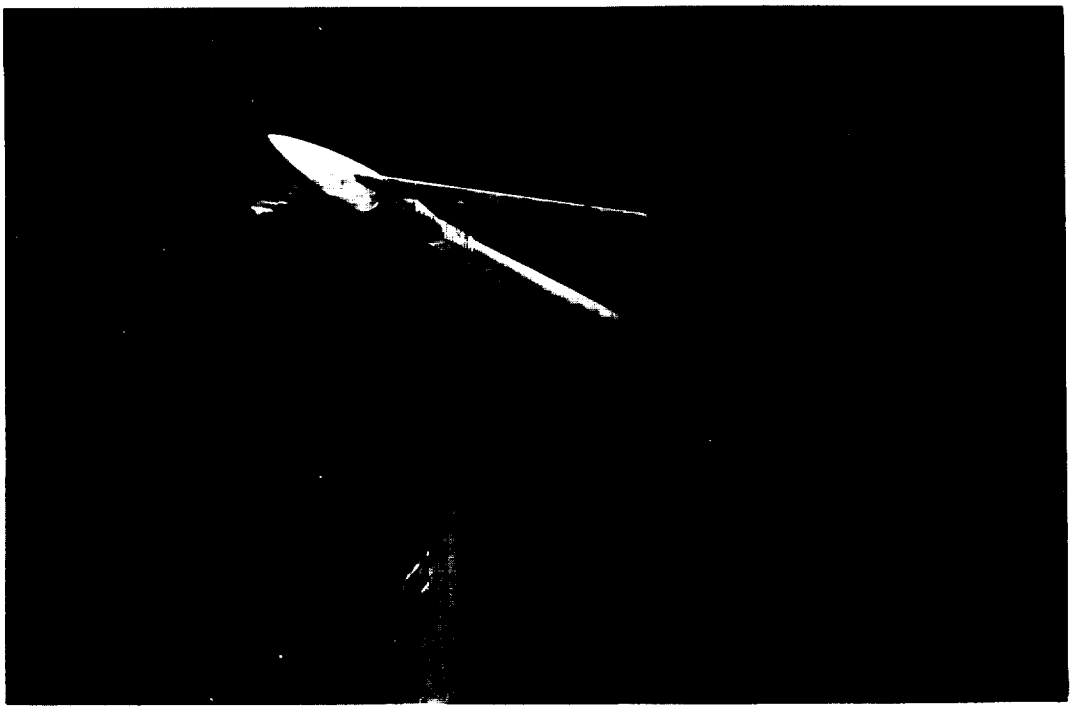

A-22308

(a) Model at $\alpha = 4^{\circ}$.

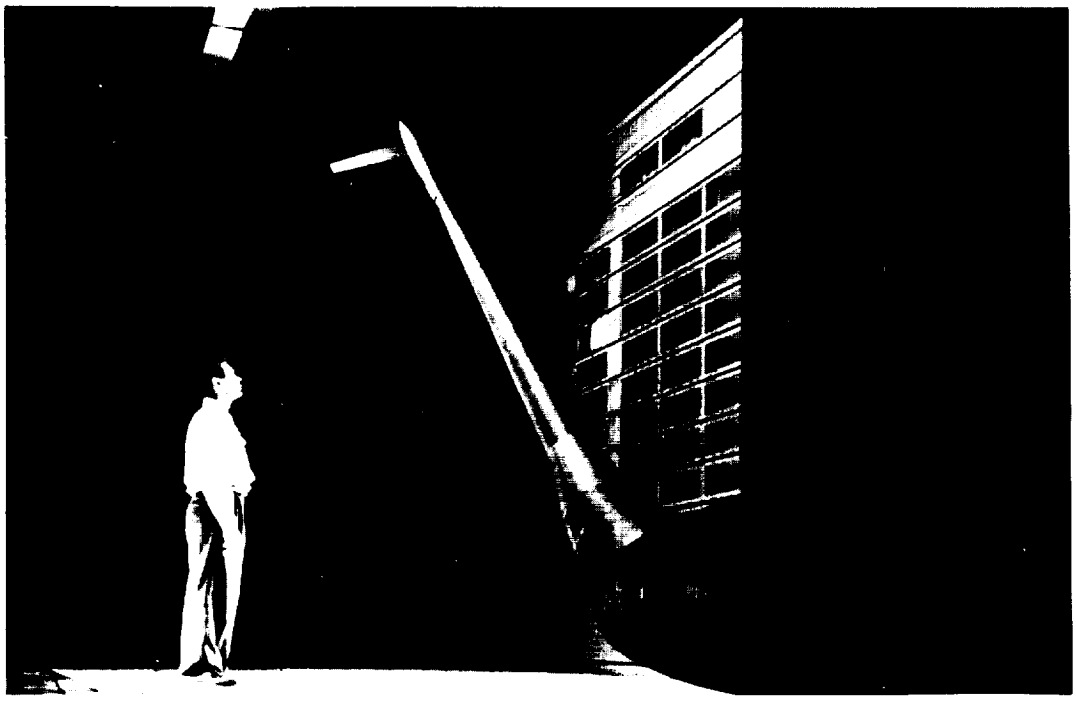

A-22309

(b) Model at $\alpha = 36^{\circ}$.

Figure 1.- Views of the model and support.

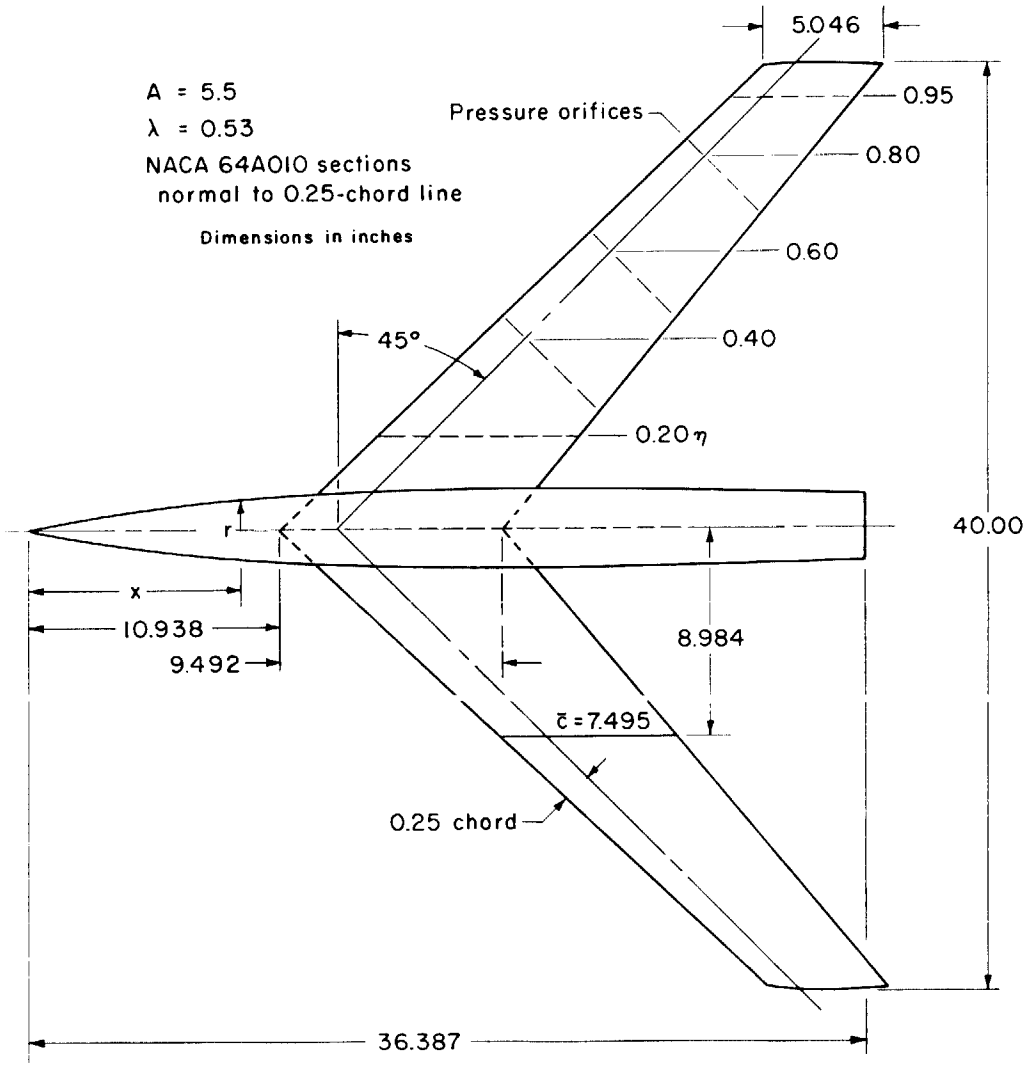

Body surface ordinates

$$r = 1.800\left[1-\left(1-\frac{x}{22.5}\right)^2\right]^{3/4}$$

x	r
0	0
2.000	0.476
4.000	0.773
6.000	1.009
8.000	1.204
10.000	1.365
12.000	1.497
14.000	1.604
16.000	1.686
18.000	1.746
20.000	1.783
22.500	1.800
24.000	1.794
26.000	1.767
28.000	1.719
30.000	1.648
32.000	1.554
34.000	1.434
36.387	1.256

Figure 2.- Dimensions of the model and locations of the orifice stations.

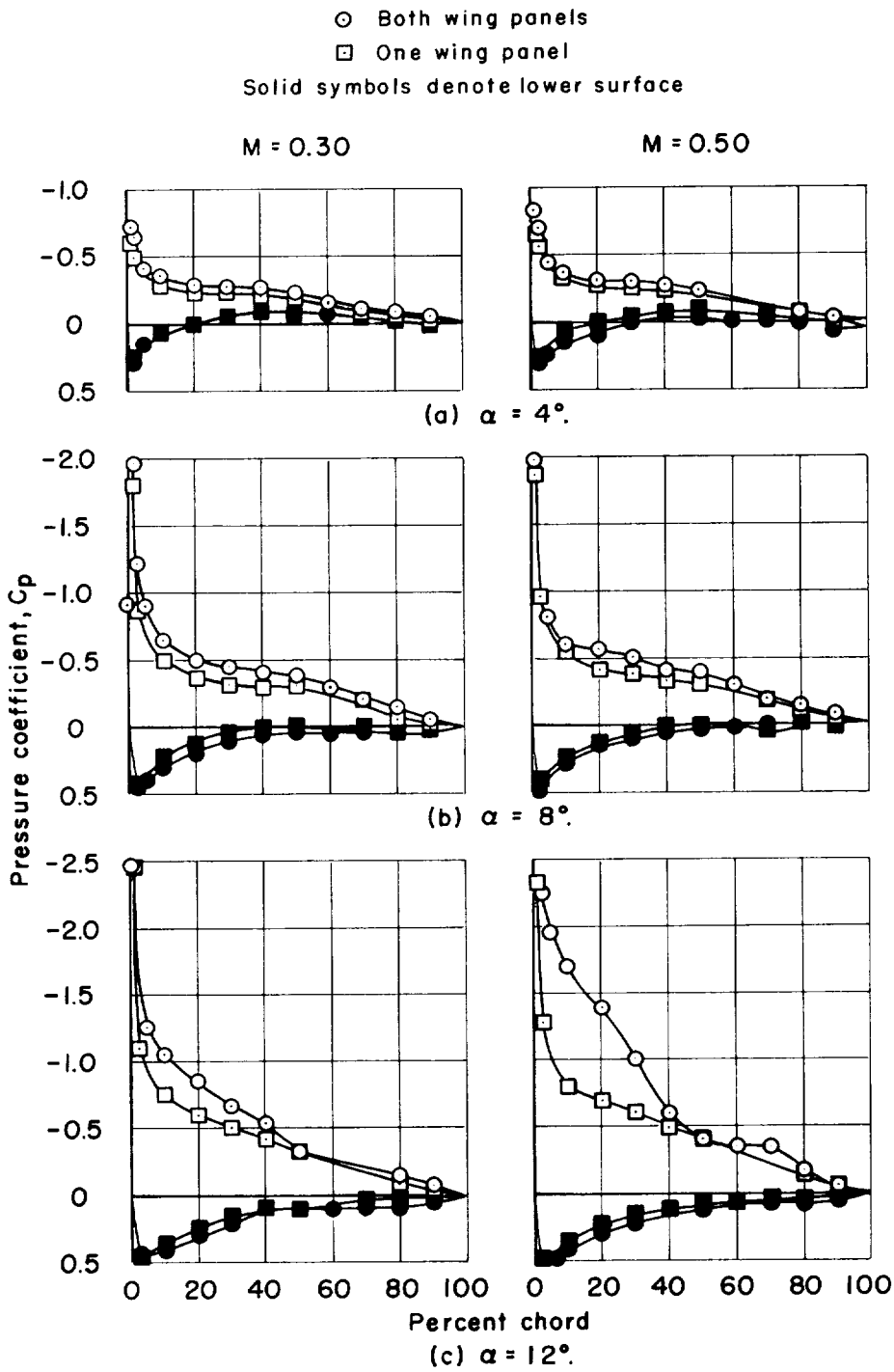

Figure 3.- Chordwise pressure distributions at $\eta = 0.20$.

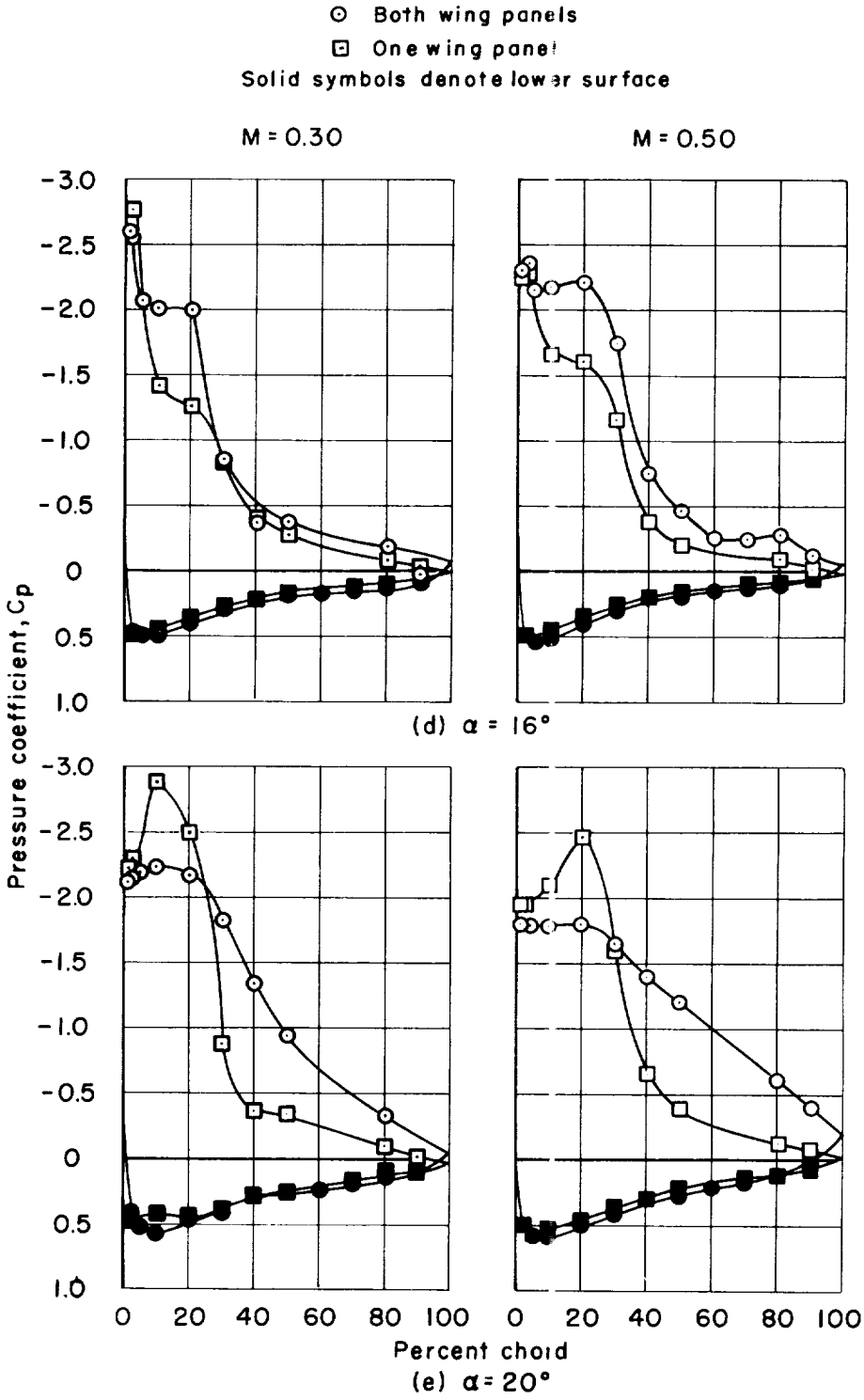

Figure 3.- Continued.

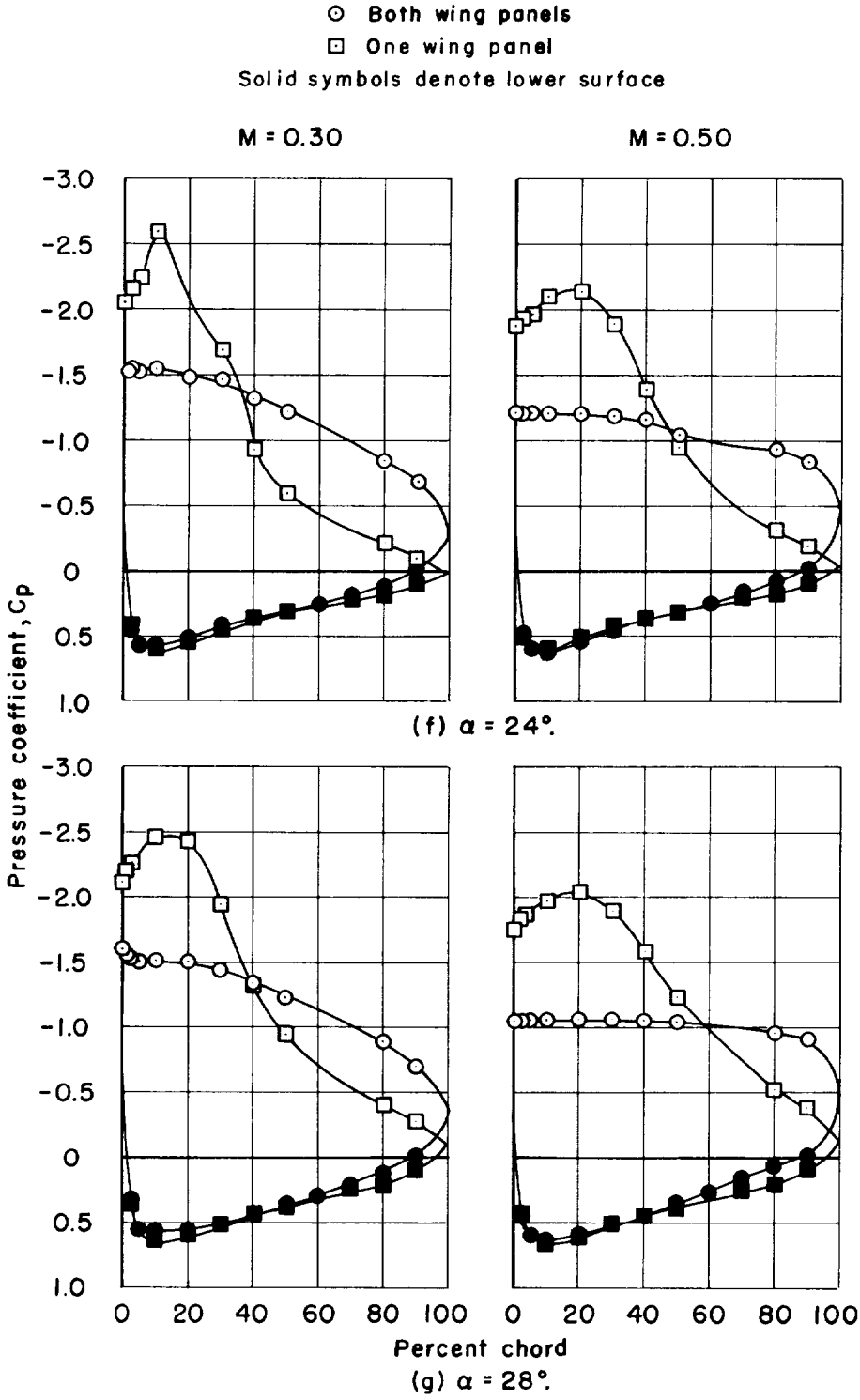

Figure 3.- Continued.

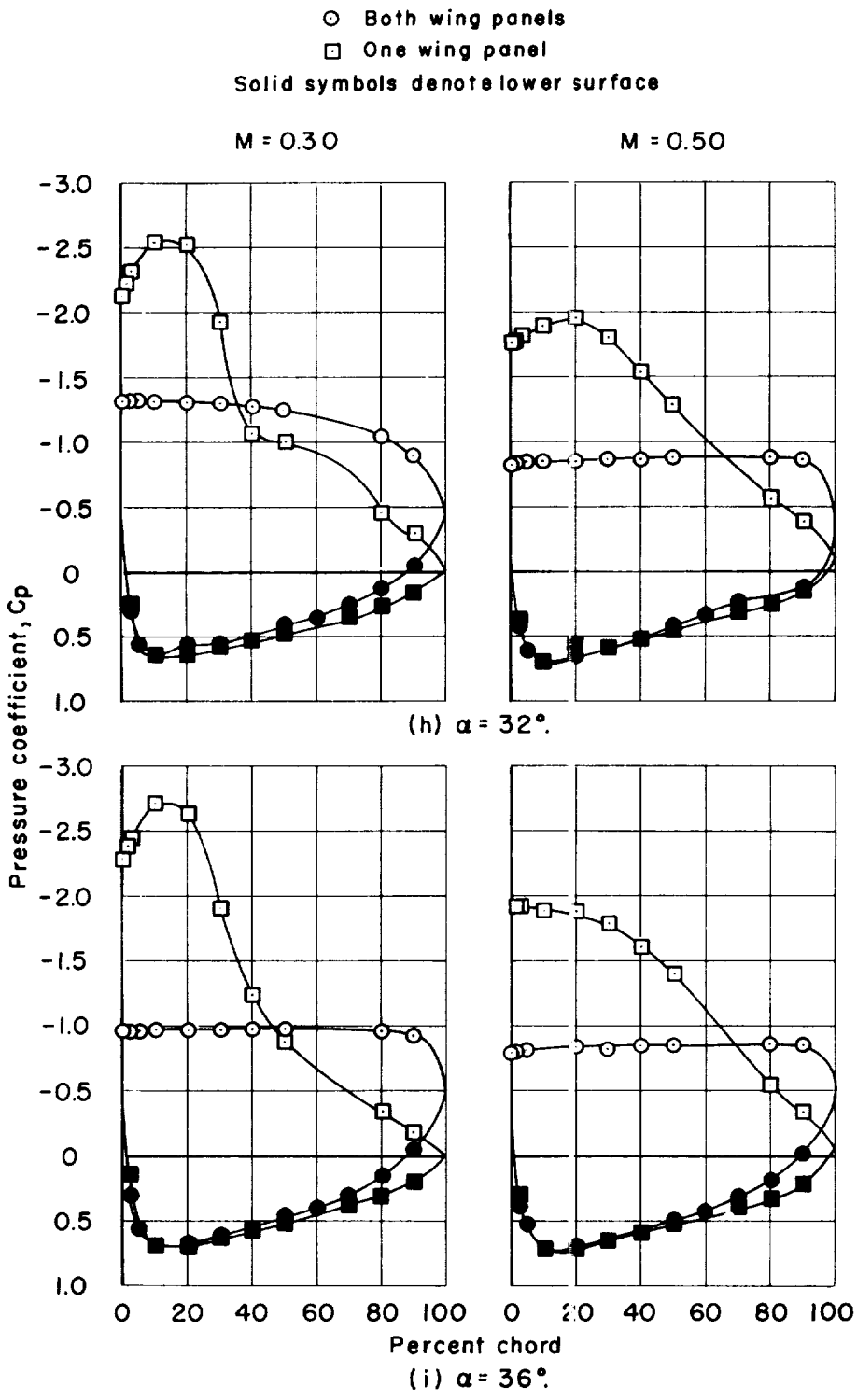

(h) $\alpha = 32°$.

(i) $\alpha = 36°$.

Figure 3.- Concluded.

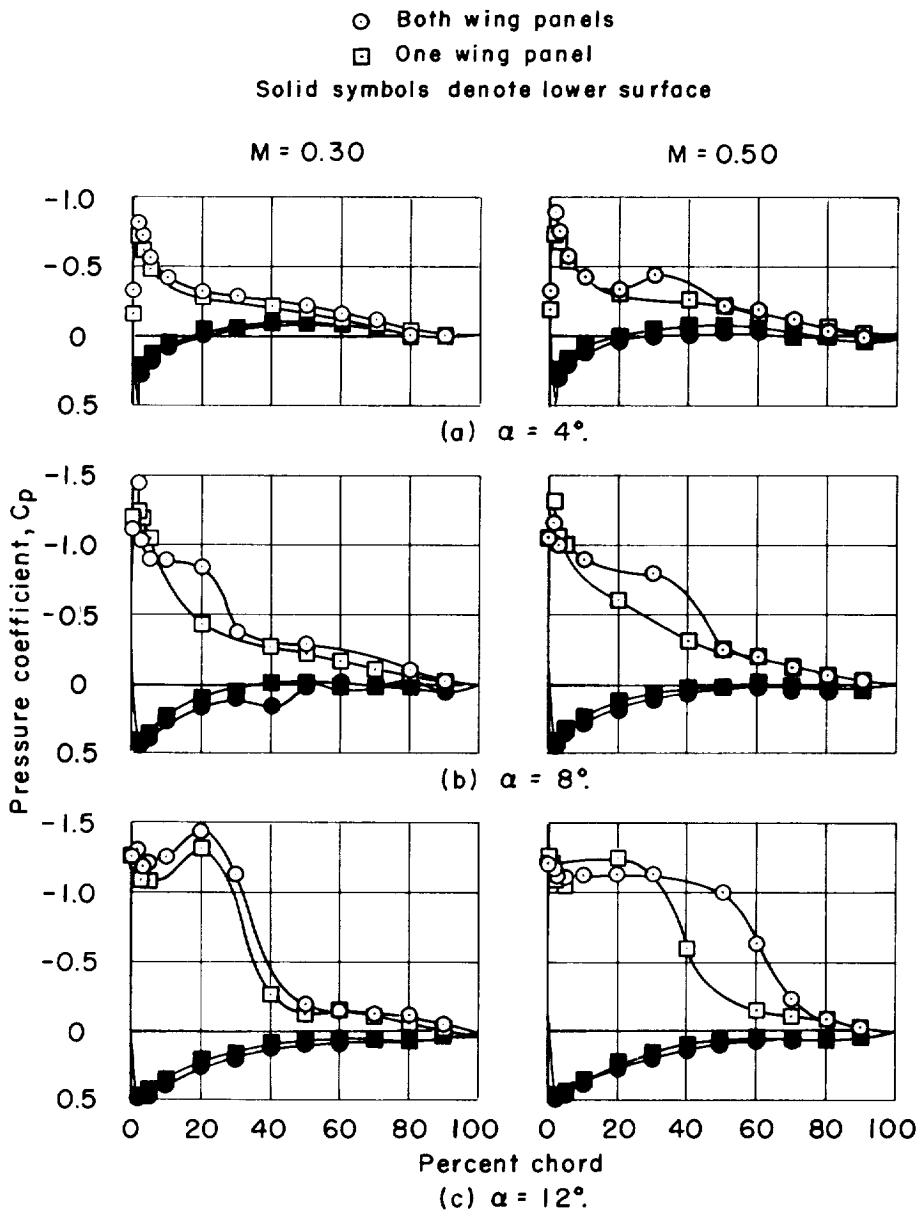

Figure 4.- Chordwise pressure distributions at $\eta = 0.40$.

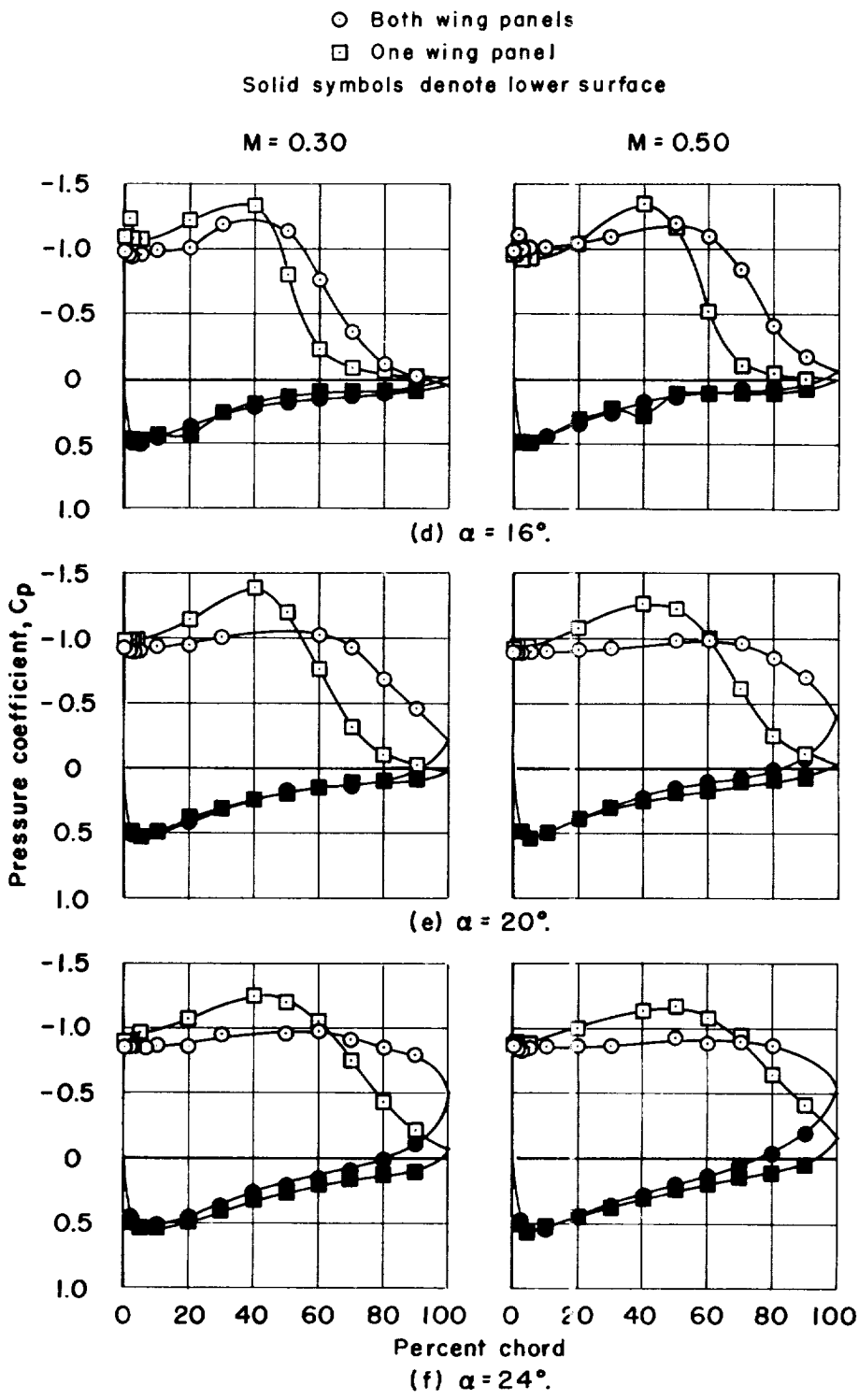

Figure 4.- Continued.

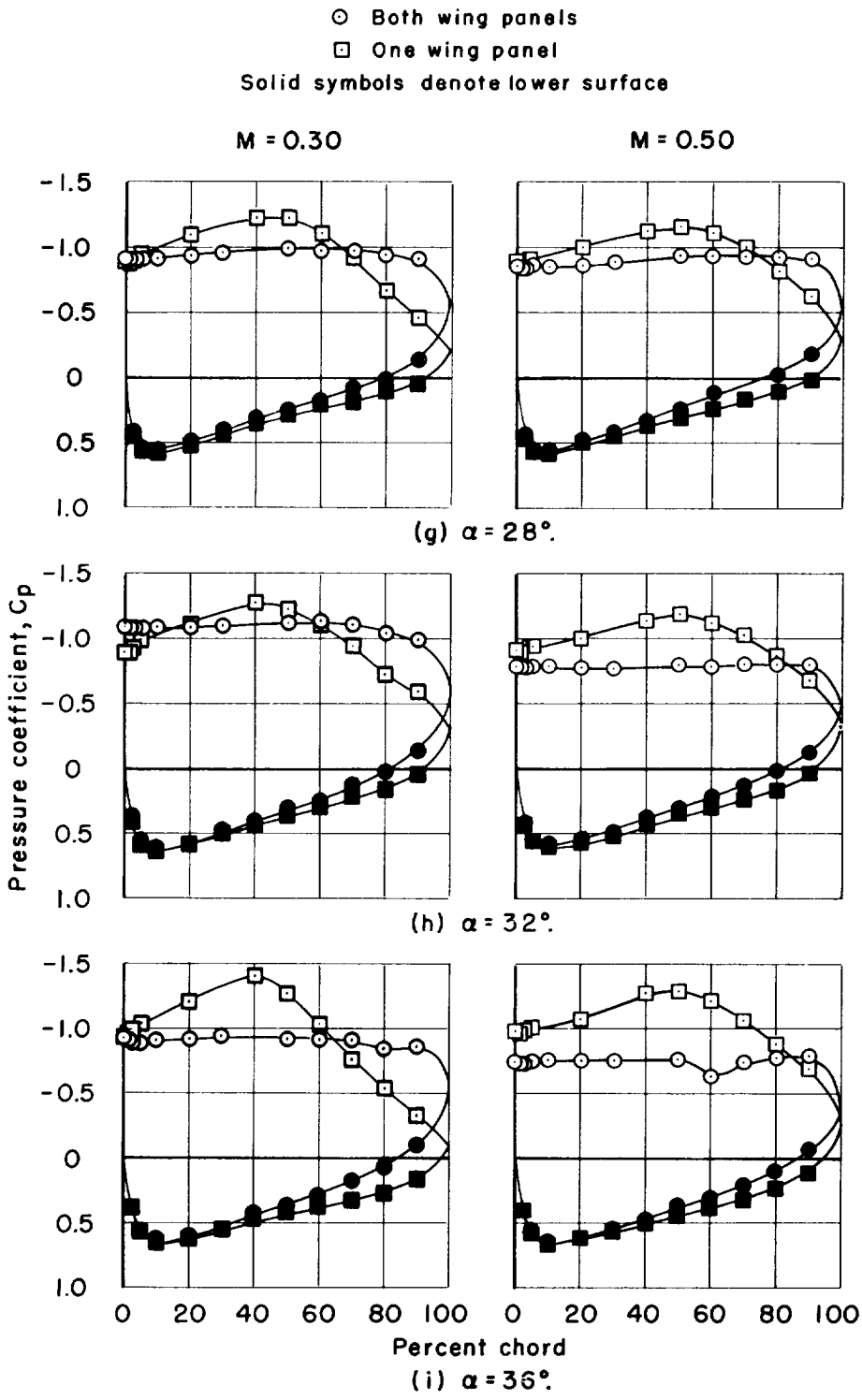

Figure 4.- Concluded.

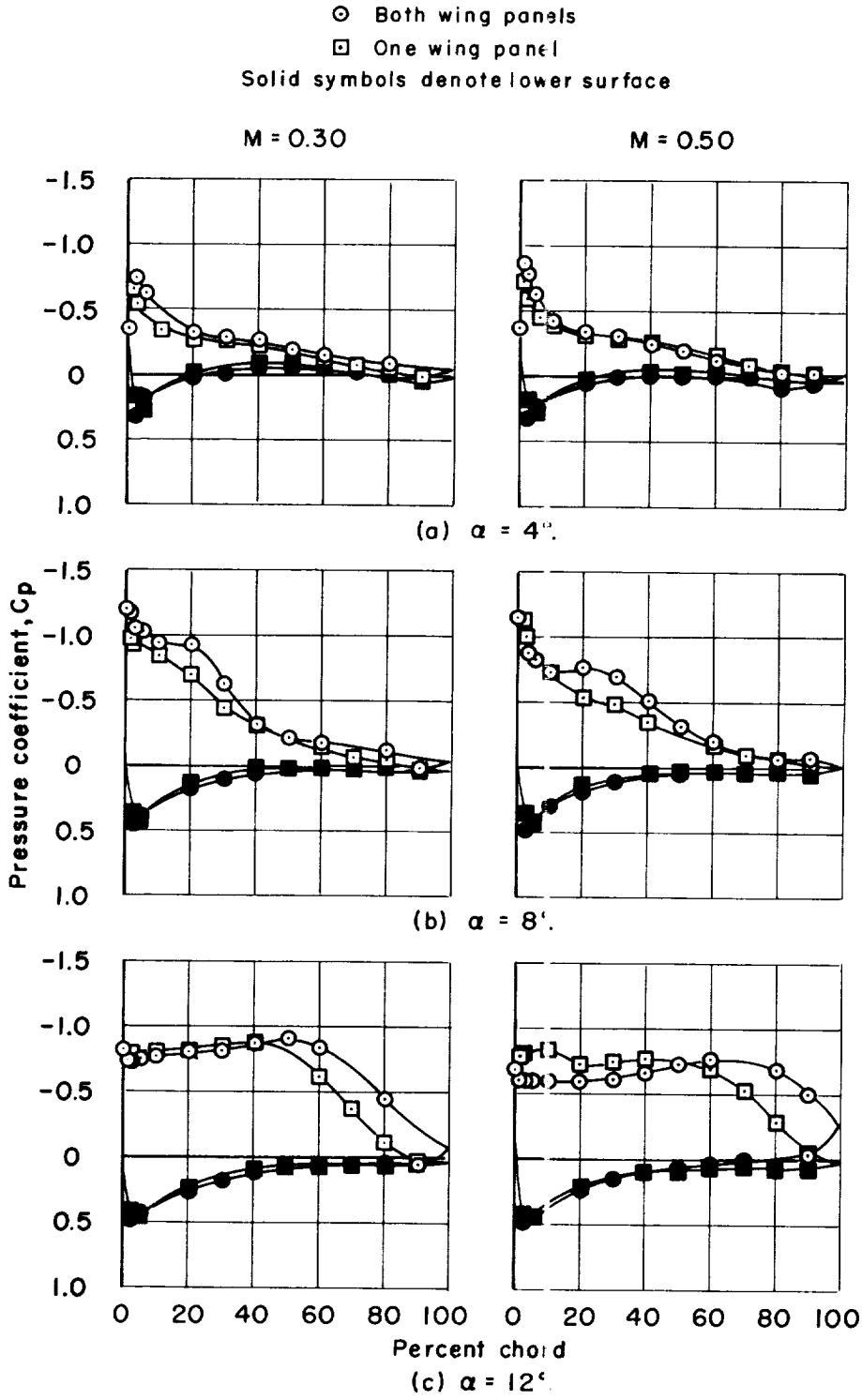

Figure 5.- Chordwise pressure distributions at $\eta = 0.60$.

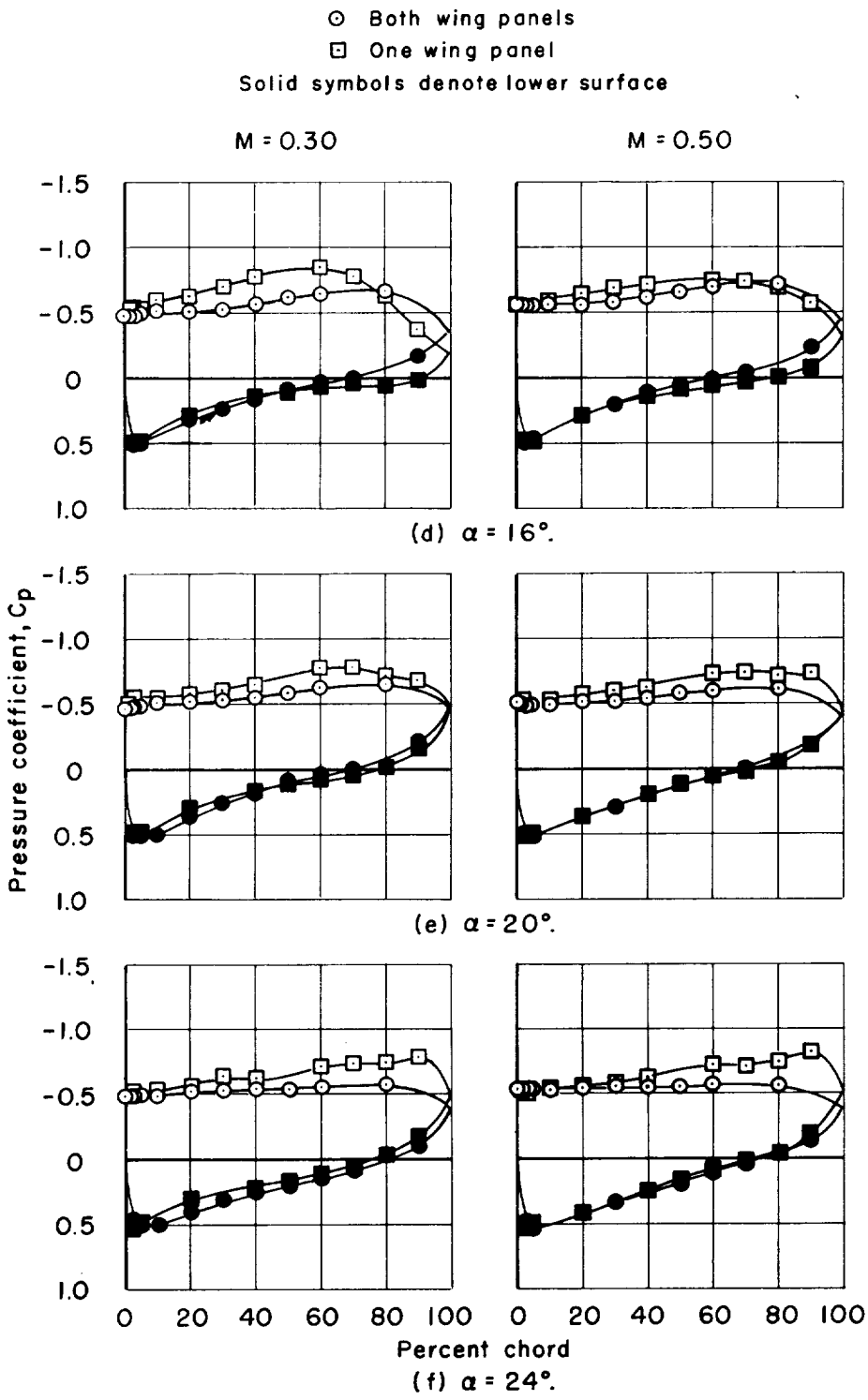

Figure 5.- Continued.

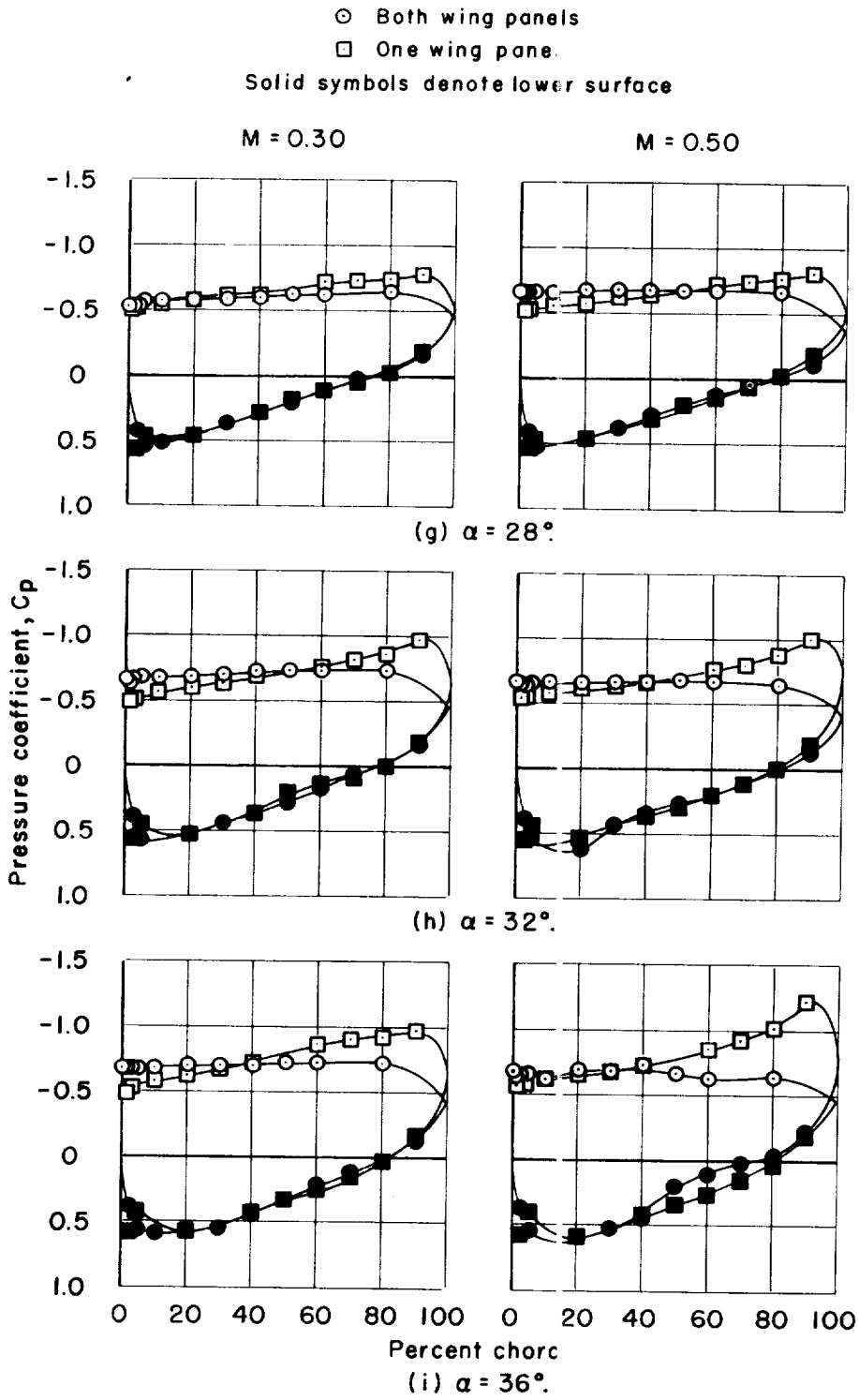

Figure 5.- Concluded.

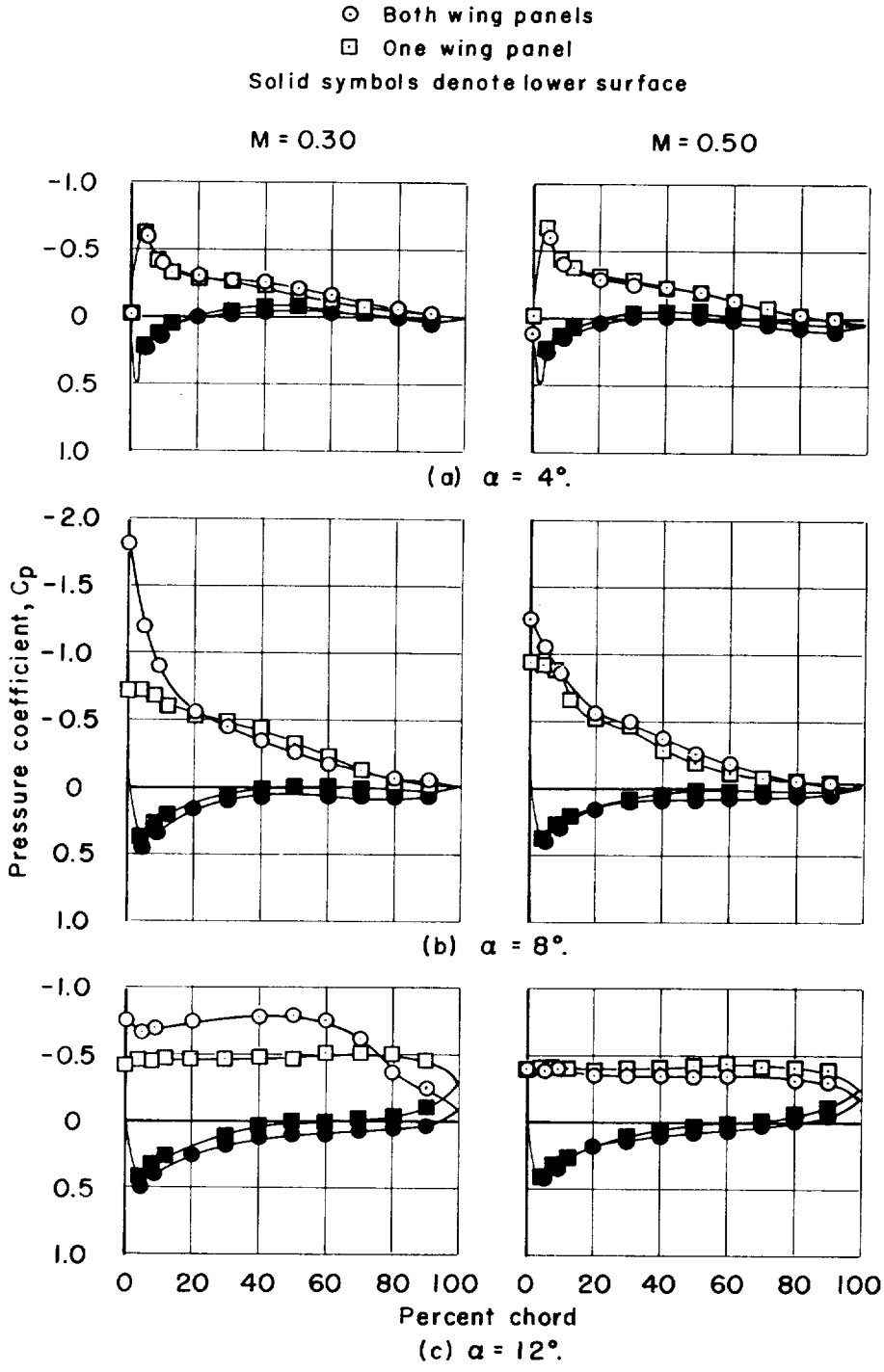

Figure 6.- Chordwise pressure distributions at $\eta = 0.80$.

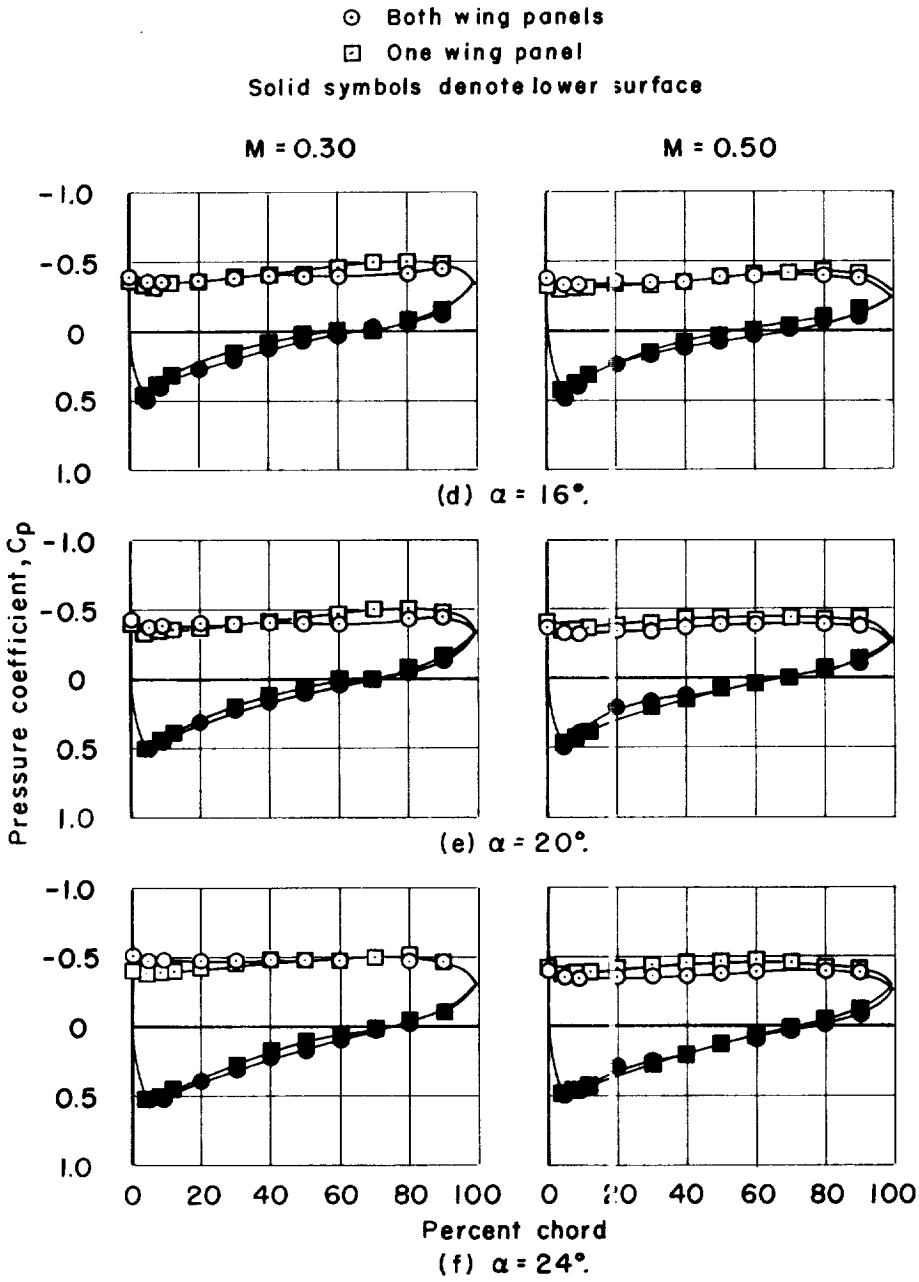

Figure 6.- Continued.

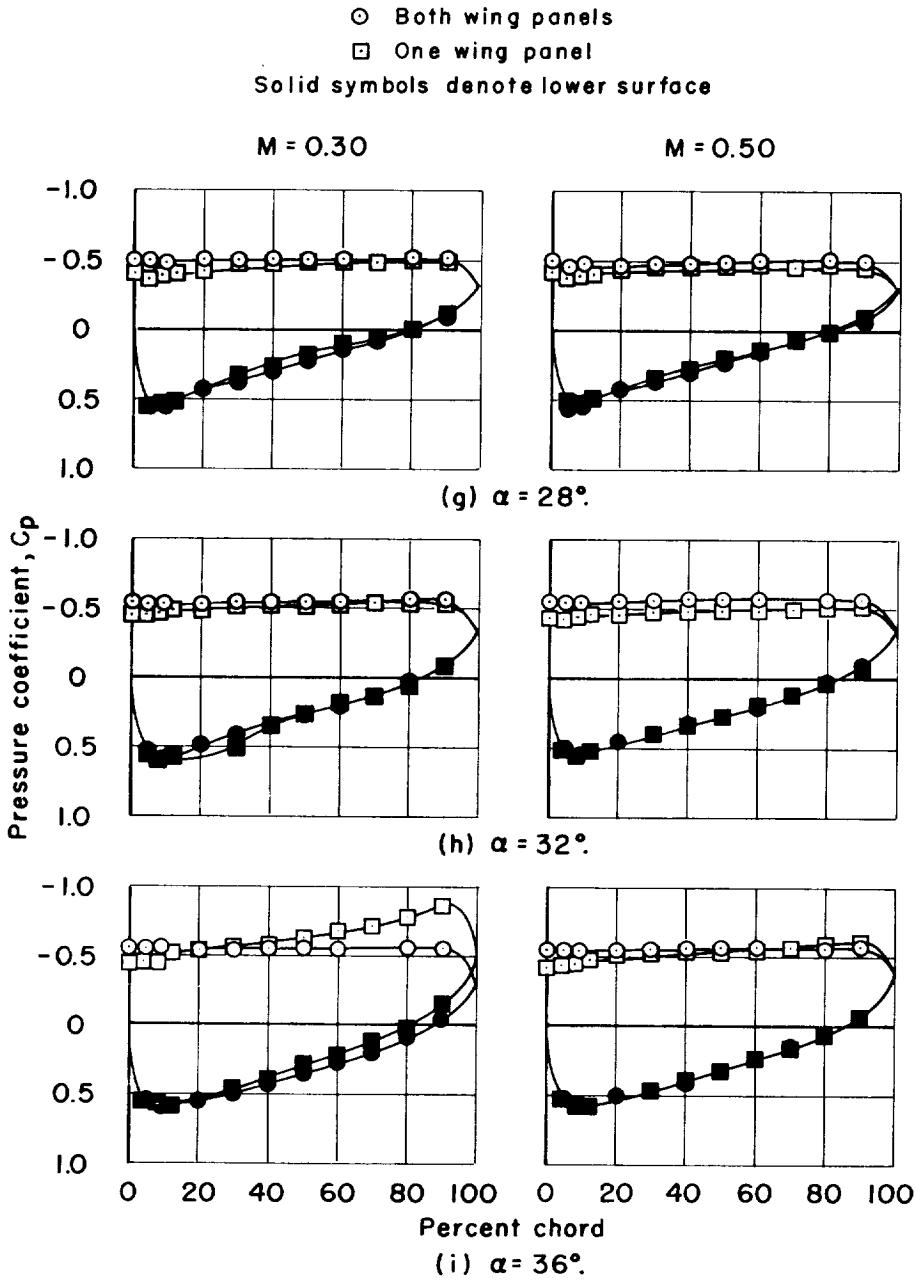

Figure 6.- Concluded.

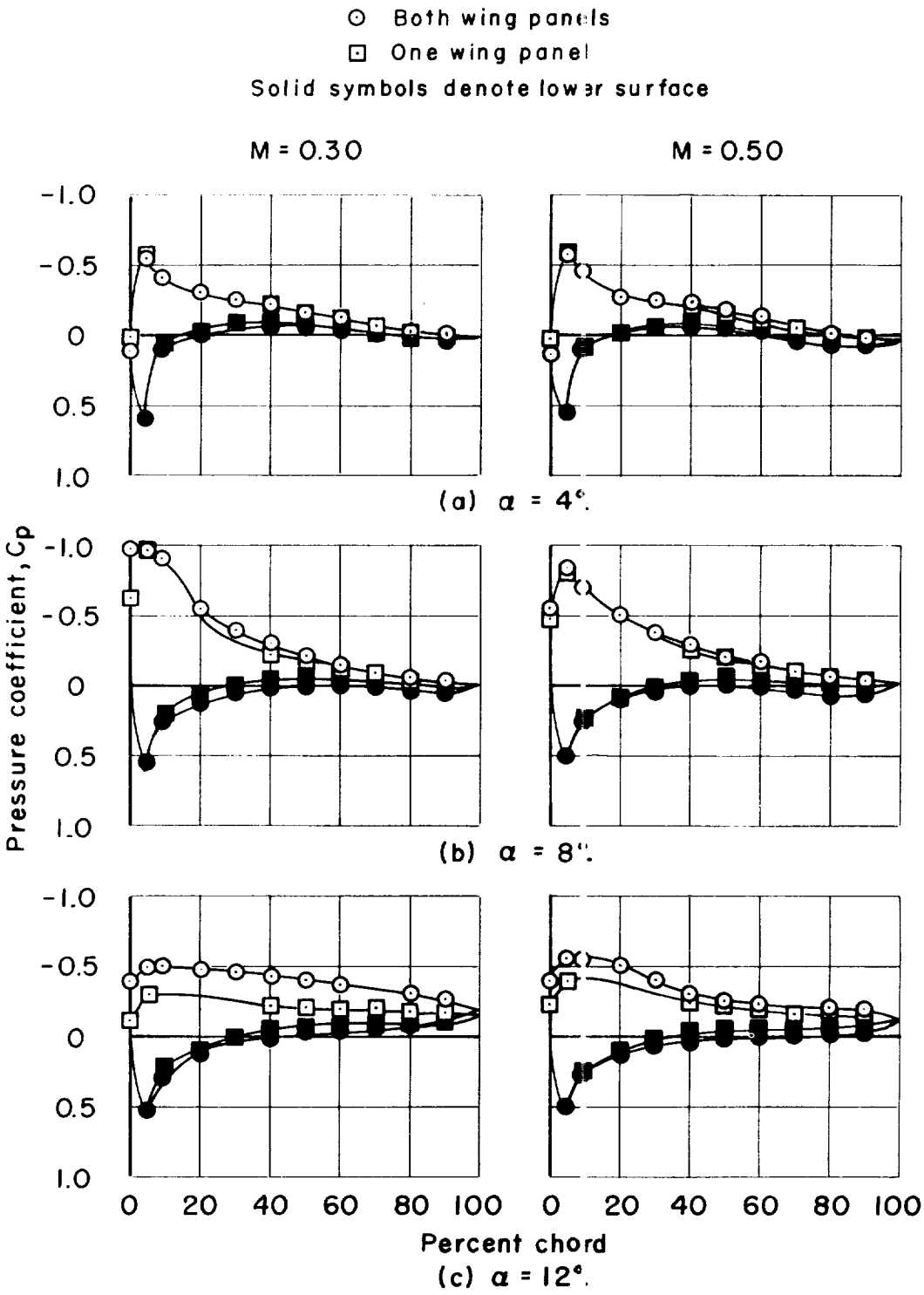

Figure 7.- Chordwise pressure distributions at $\eta = 0.95$.

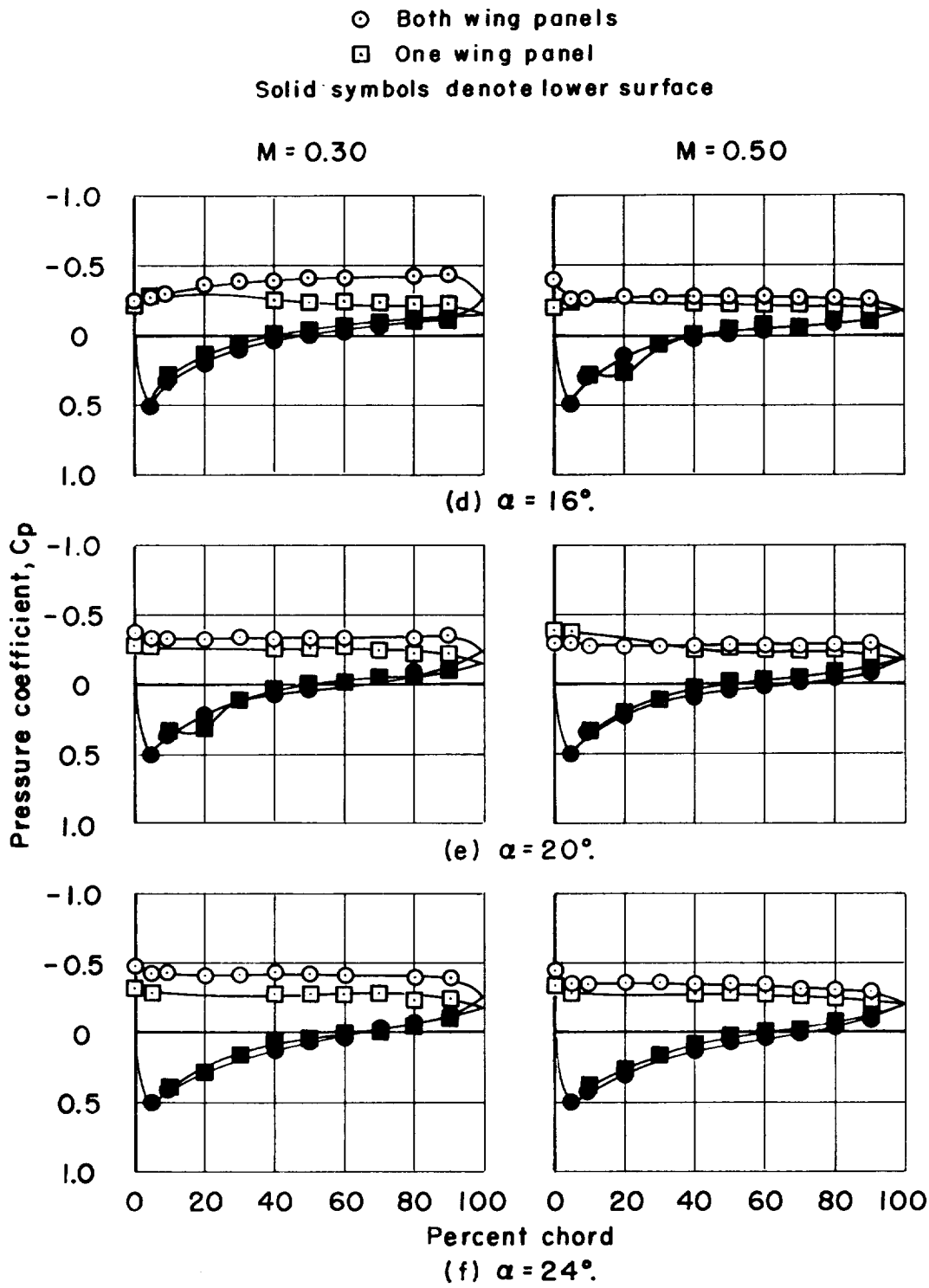

Figure 7.- Continued.

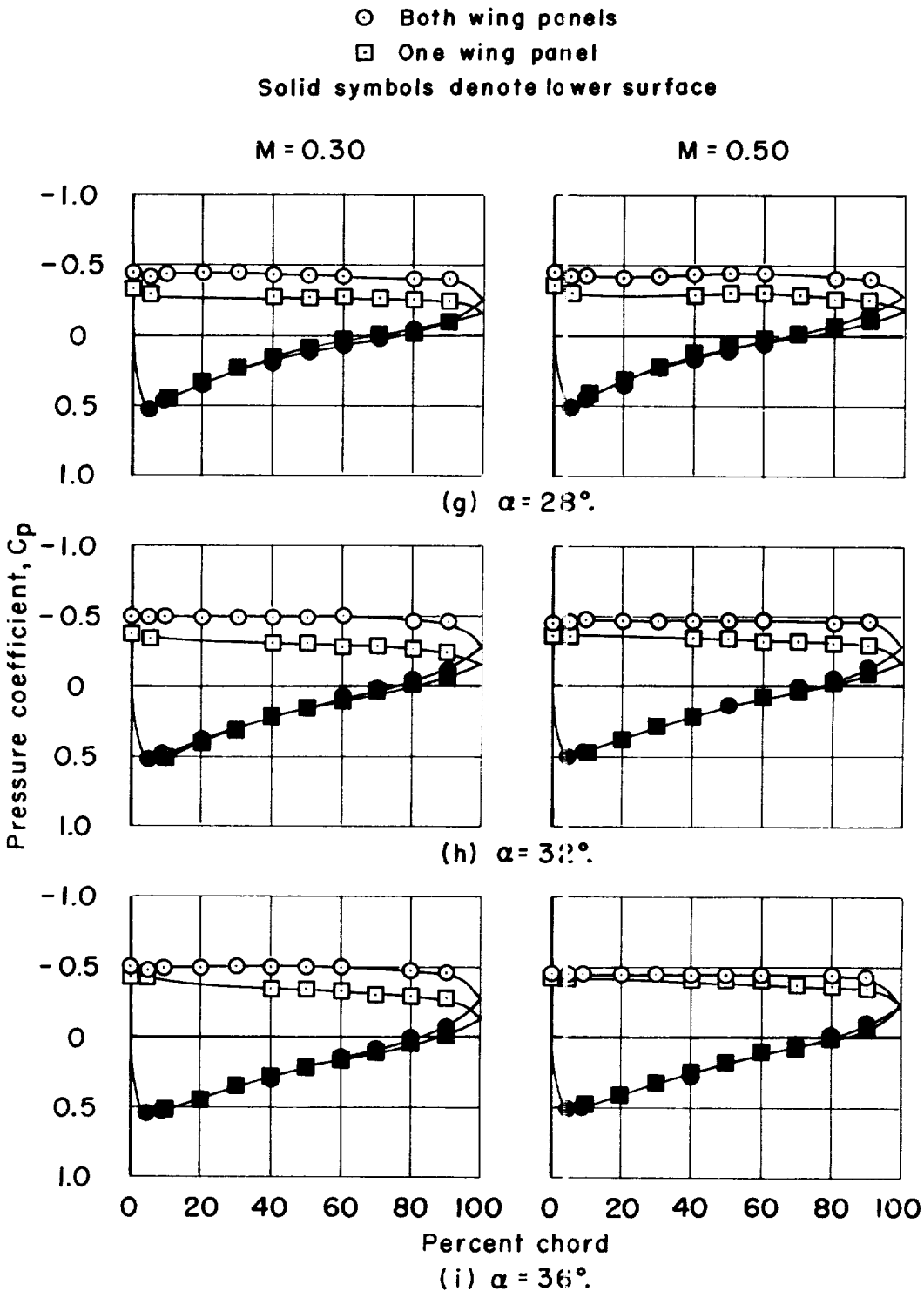

Figure 7.- Concluded.

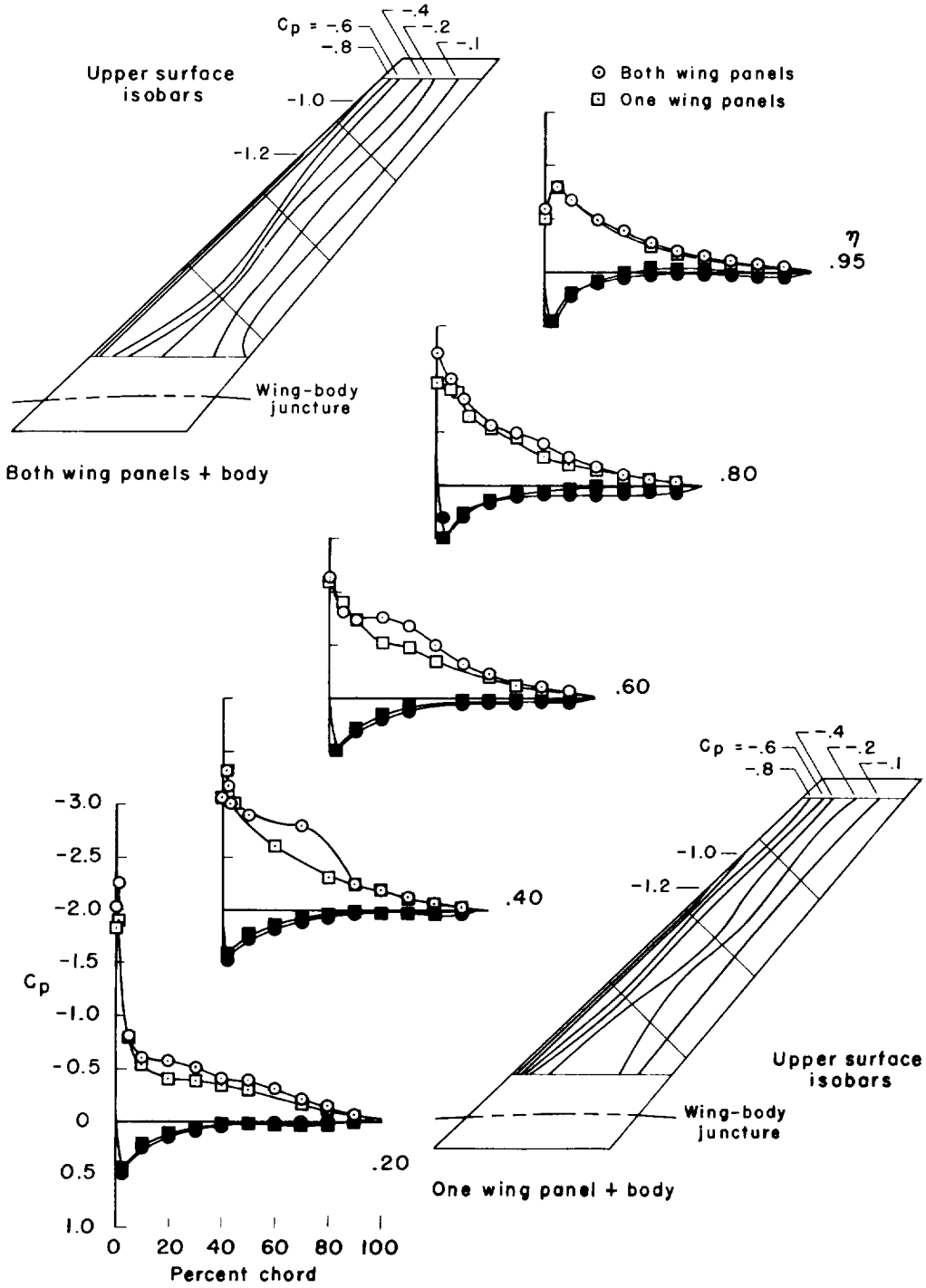

(a) $\alpha = 8°$

Figure 8.- Pressure distributions and upper surface isobars; M = 0.50.

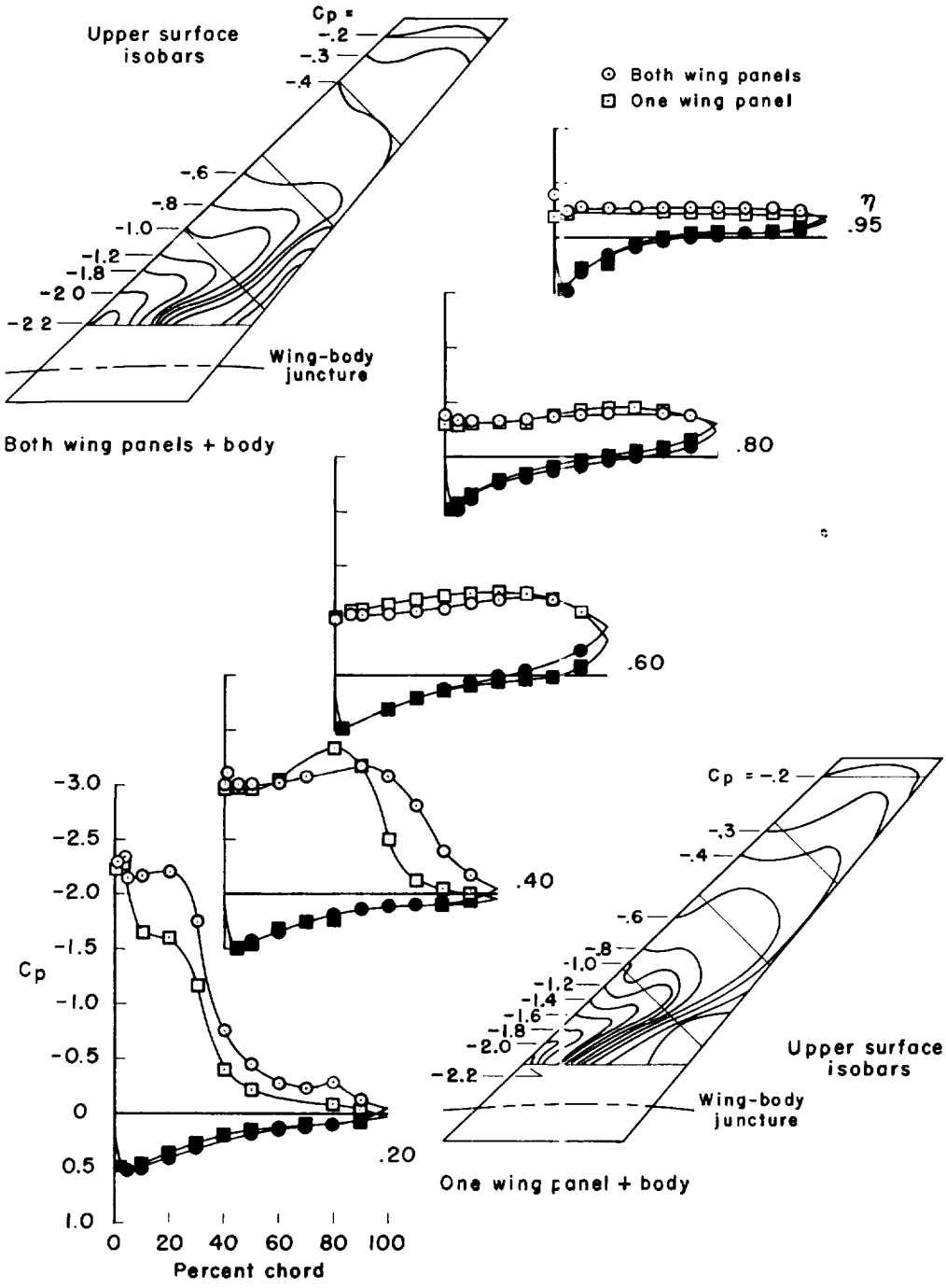

(b) $\alpha = 16°$

Figure 8.- Continued.

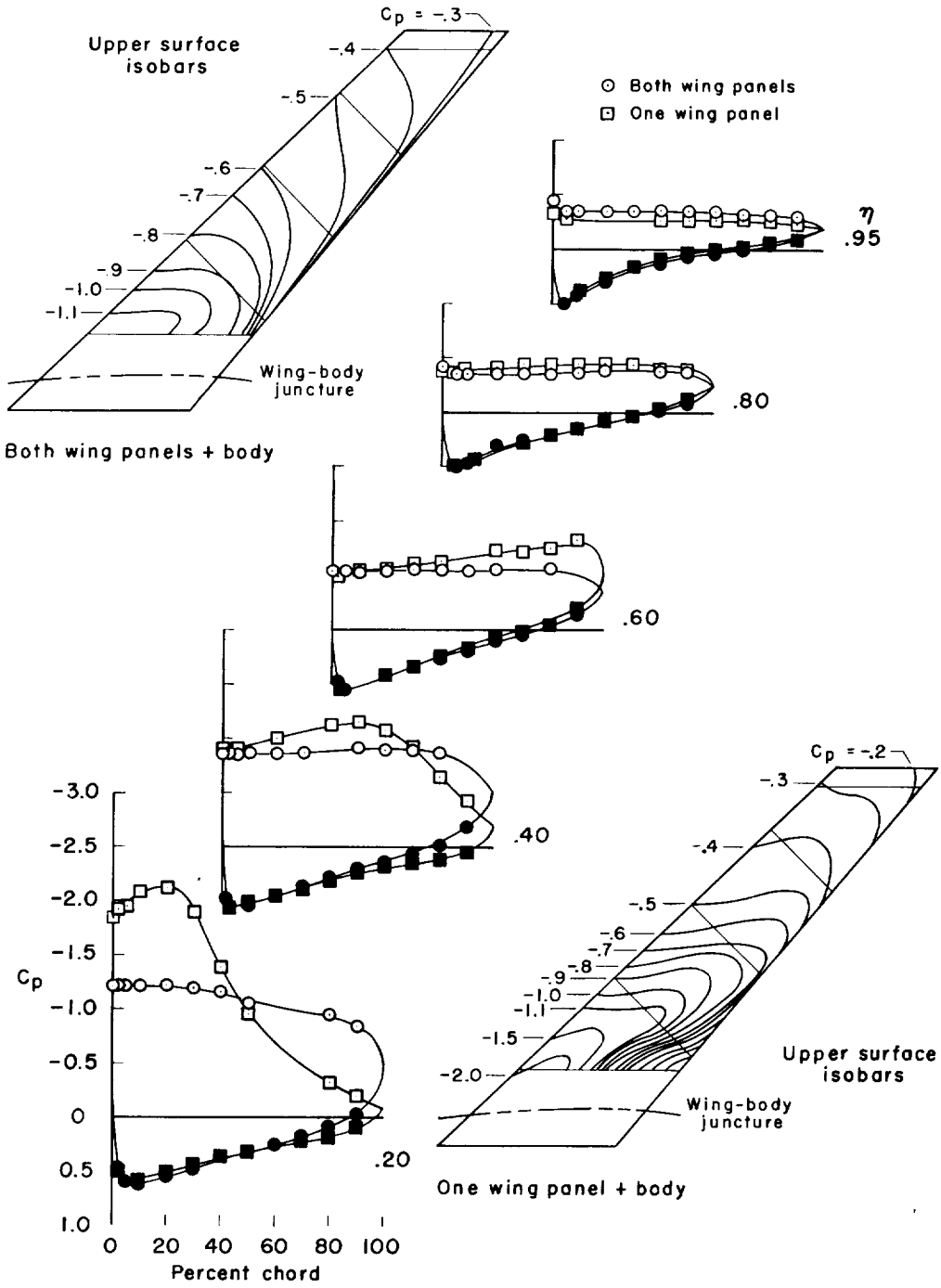

(c) $\alpha = 24°$

Figure 8.- Continued.

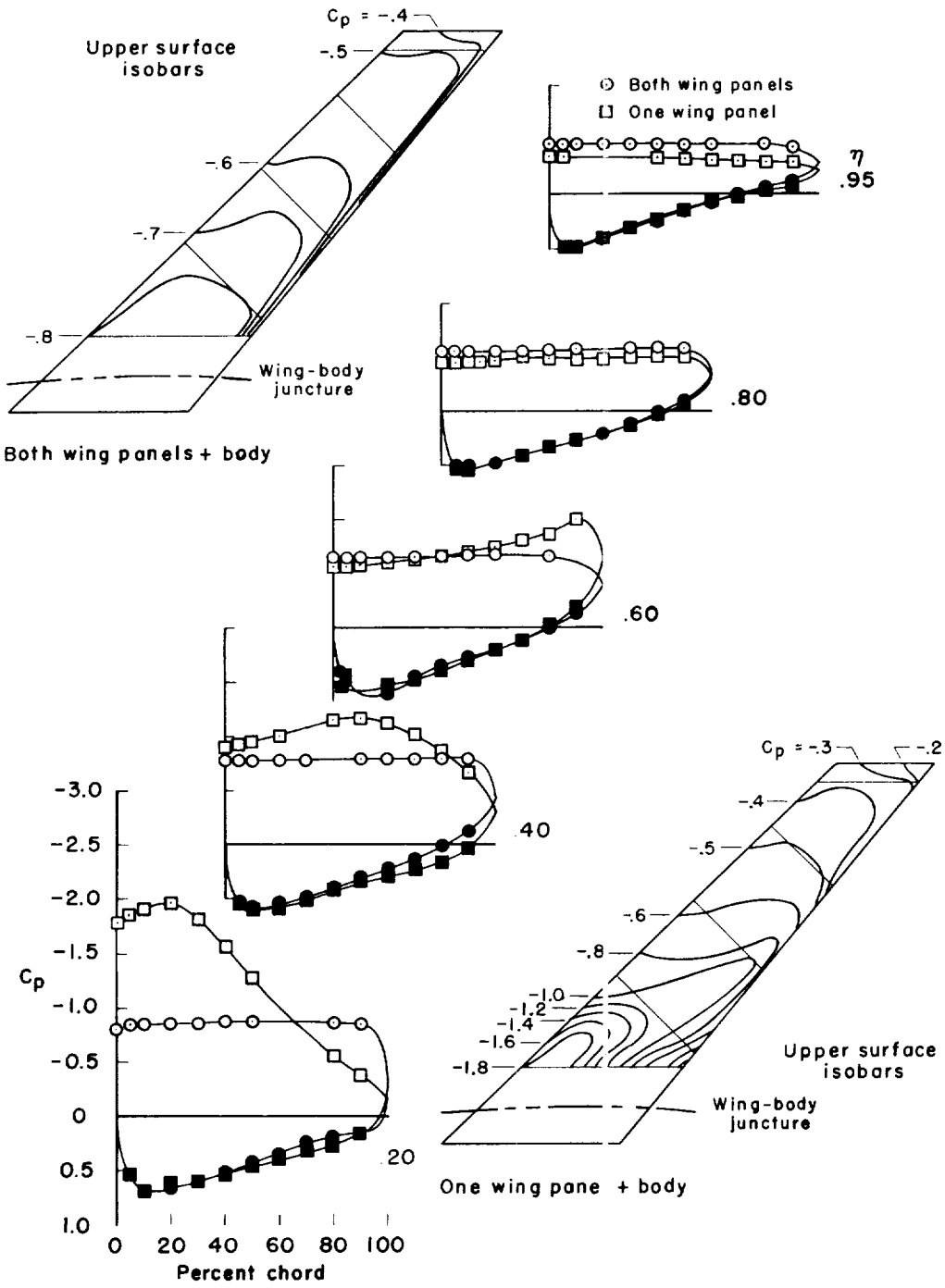

(d) $\alpha = 32°$

Figure 8.- Concluded.

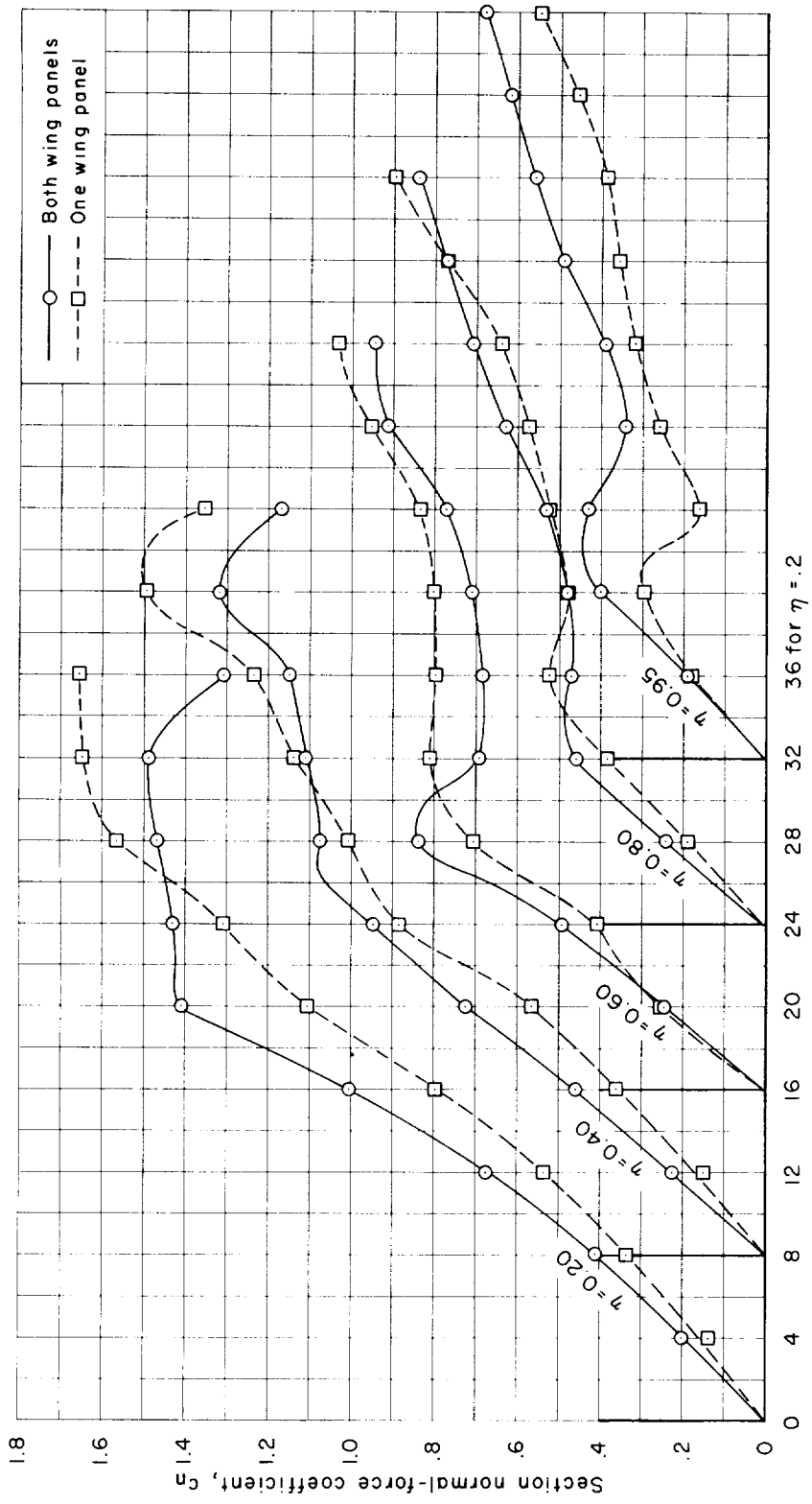

(a) M = 0.30.

Figure 9.- Variation of section normal-force coefficient with angle of attack.

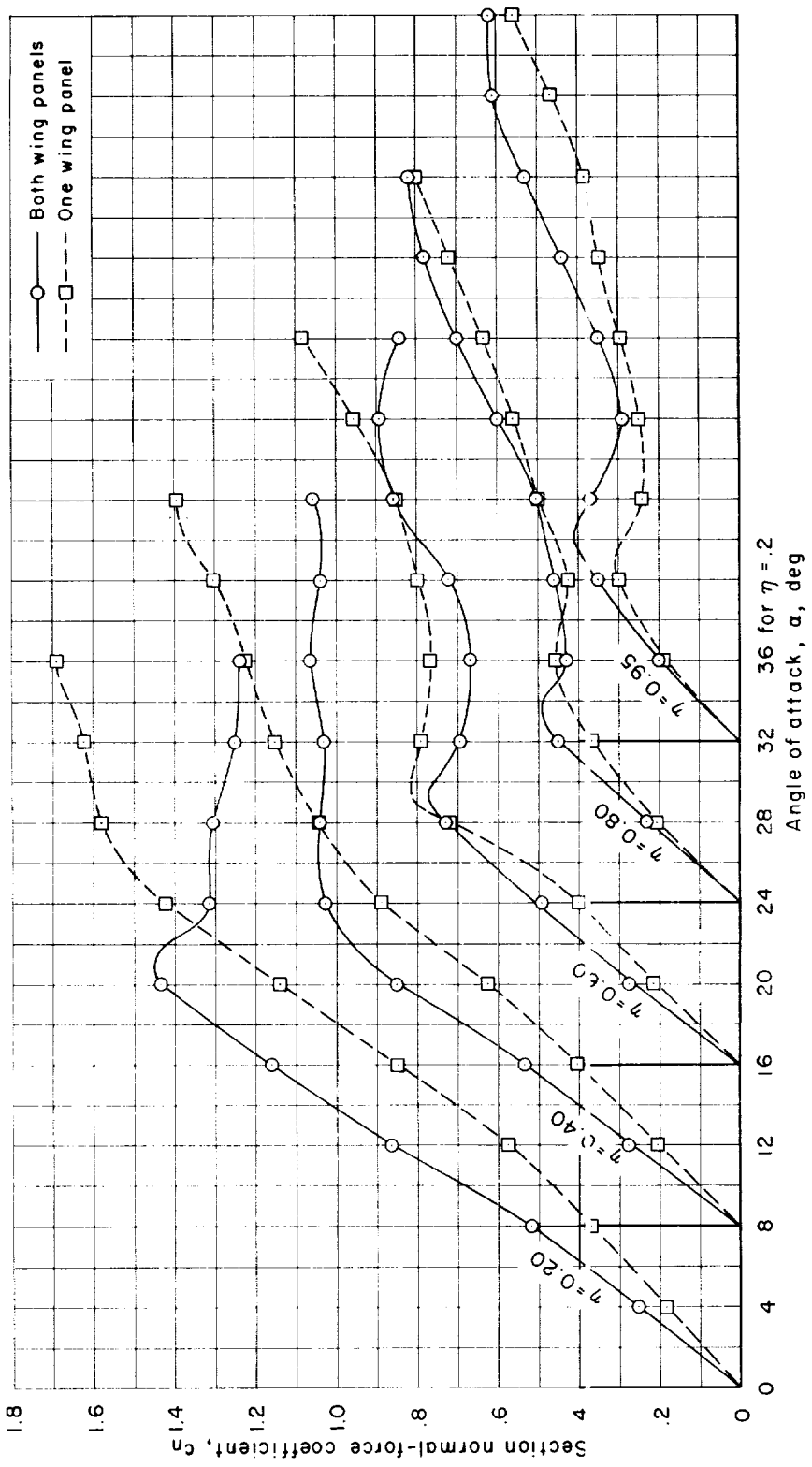

(b) M = 0.50.

Figure 9.- Concluded.

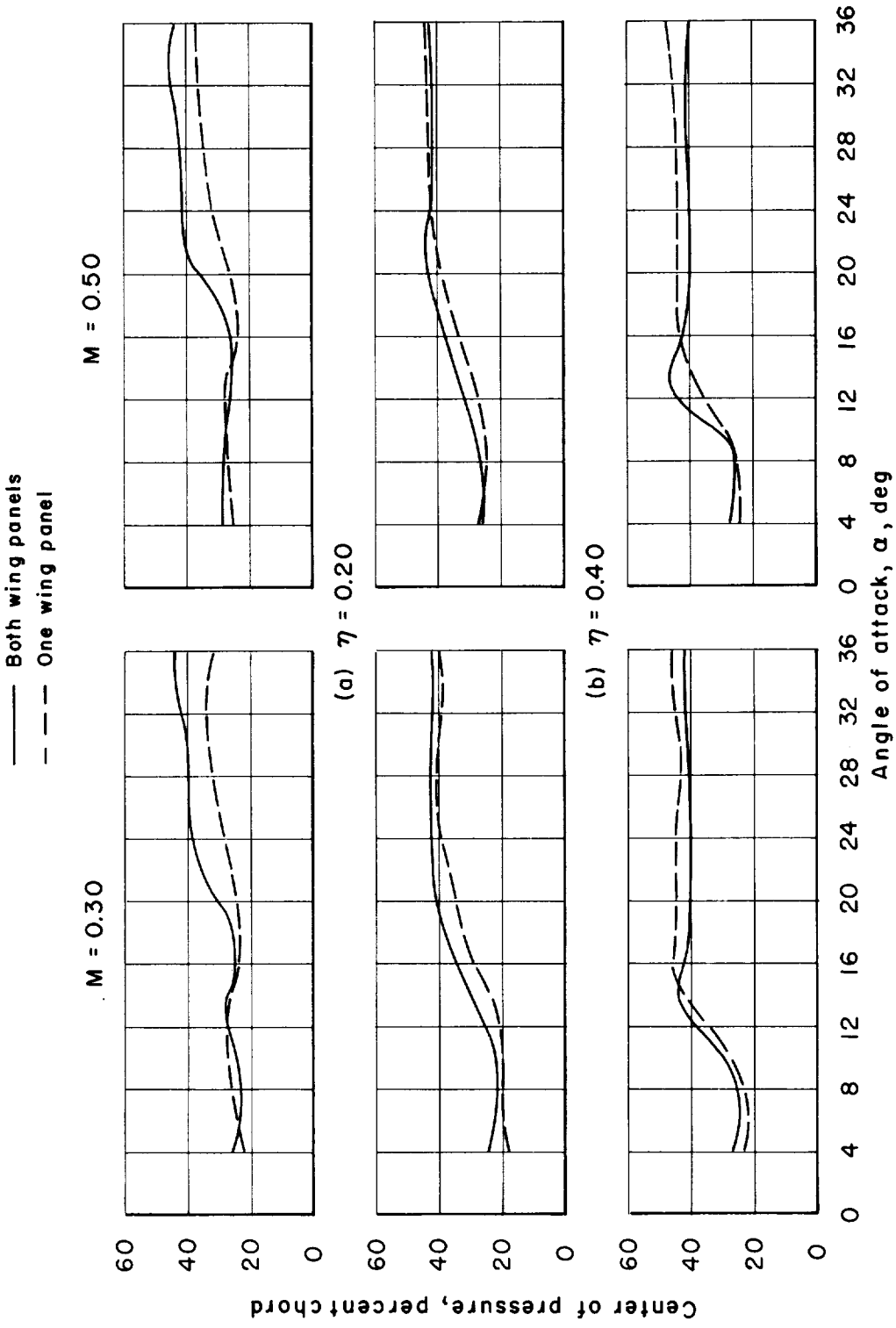

Figure 10.- Variation with angle of attack of the chordwise locations of the section centers of pressure.

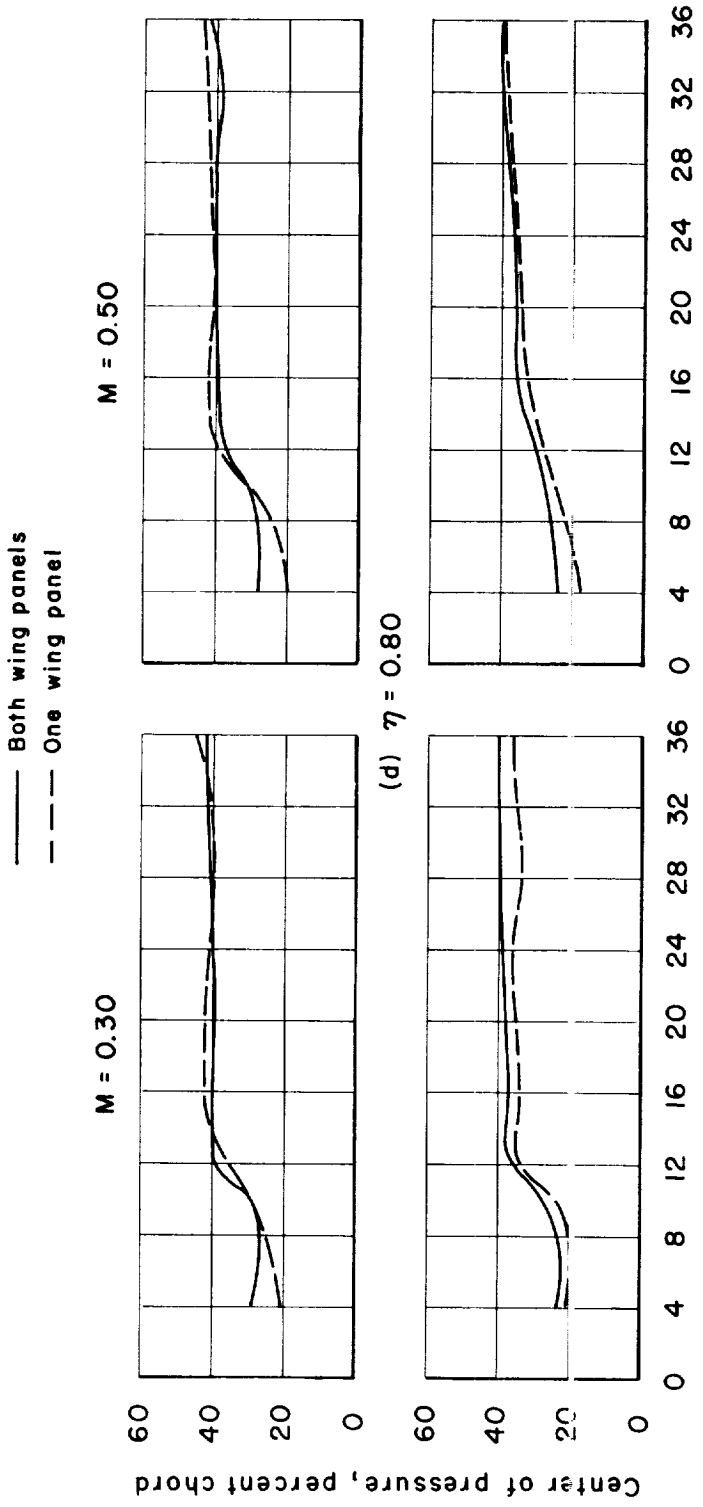

Figure 10.- Concluded.

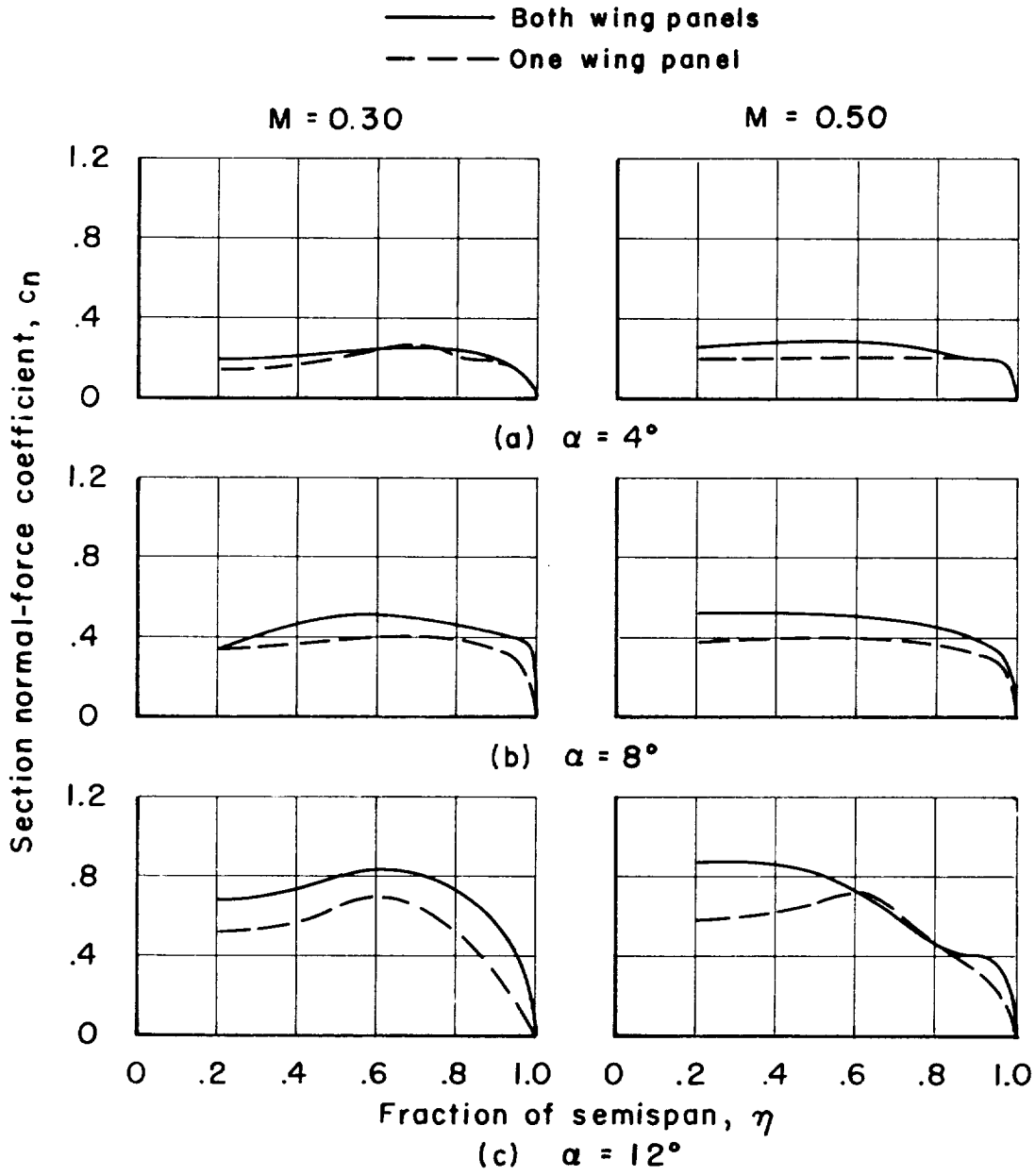

Figure 11.- Spanwise variations of section normal-force coefficient at constant angles of attack.

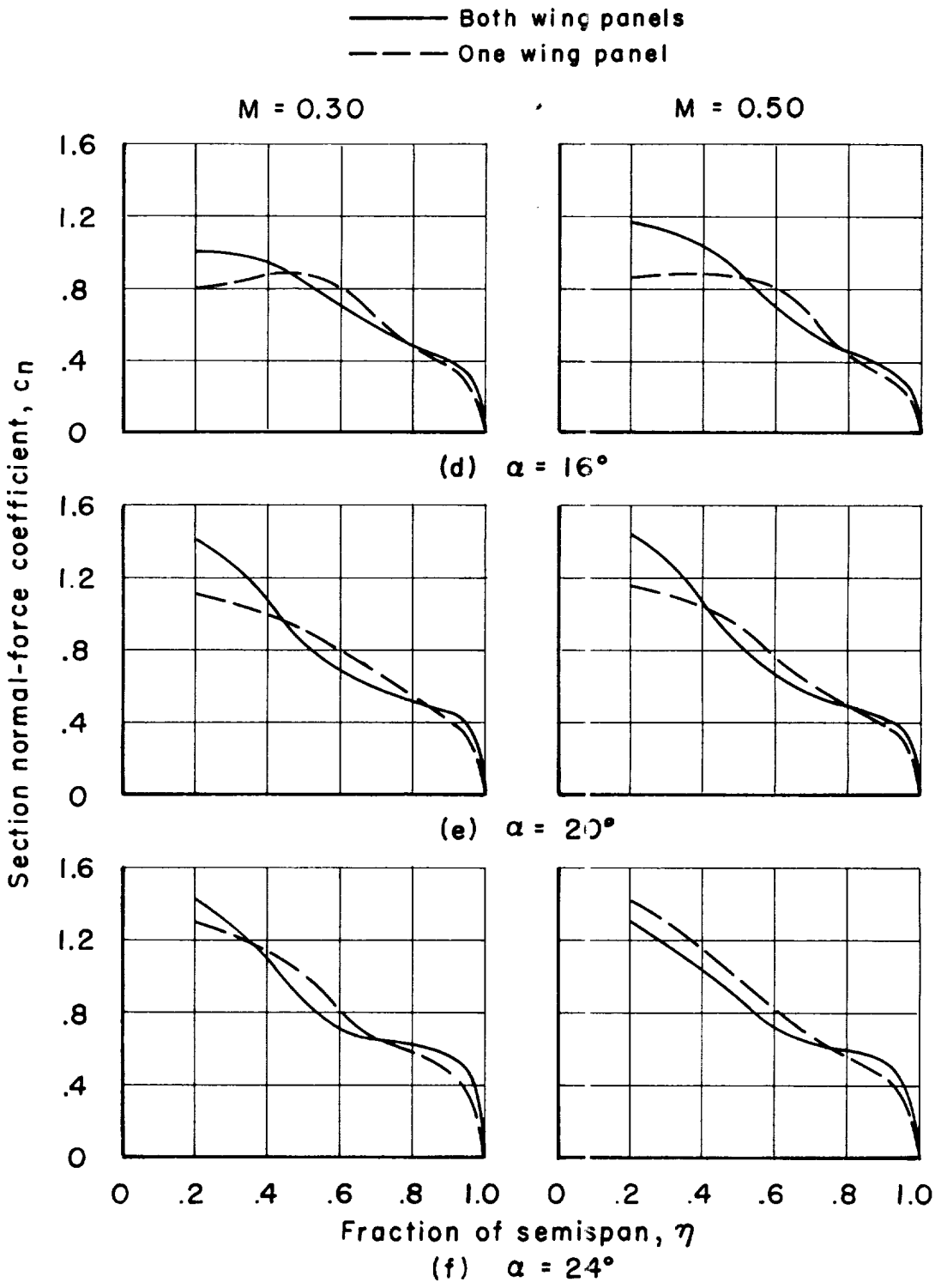

Figure 11.- Continued.

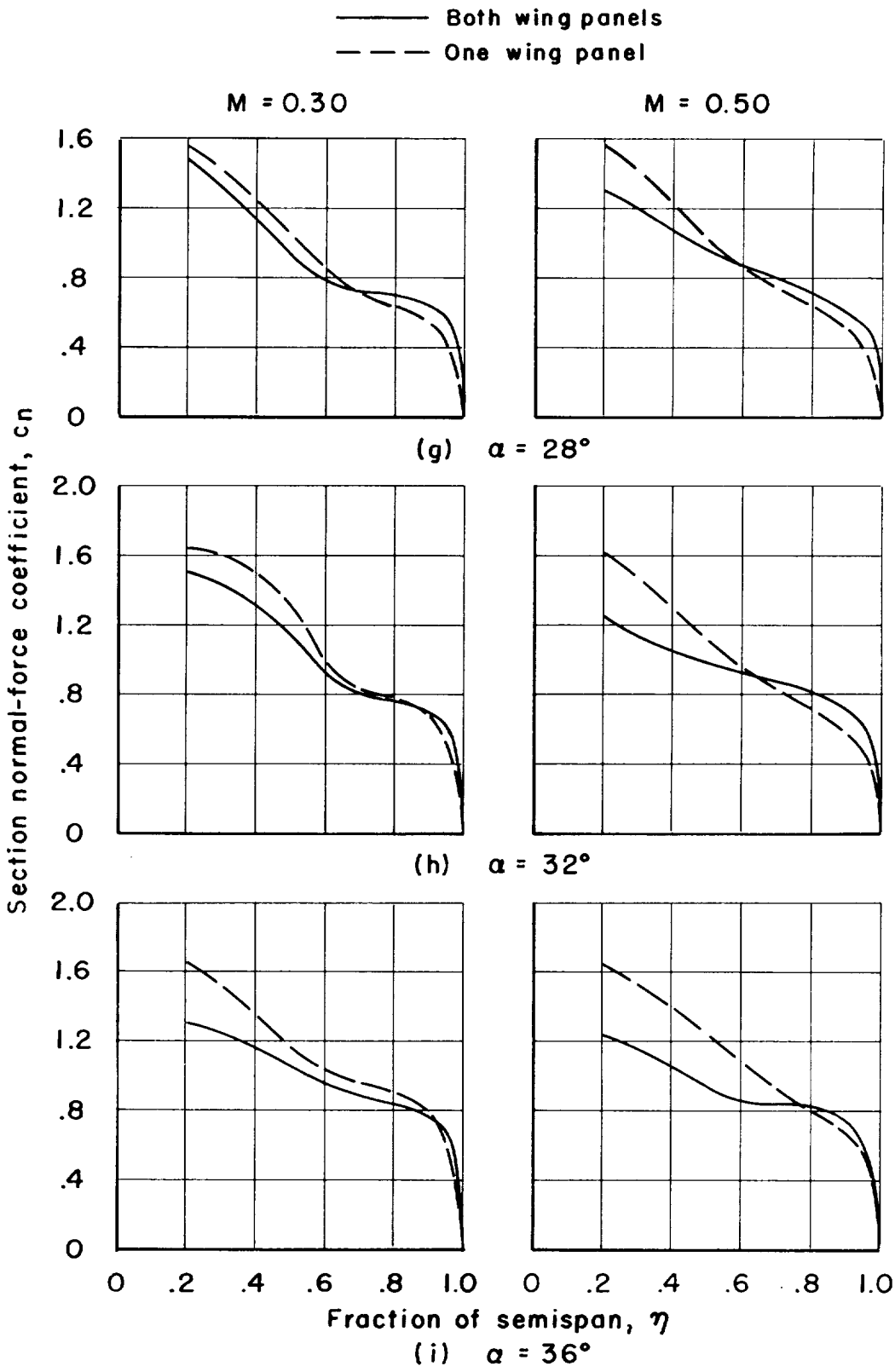

Figure 11.- Concluded.

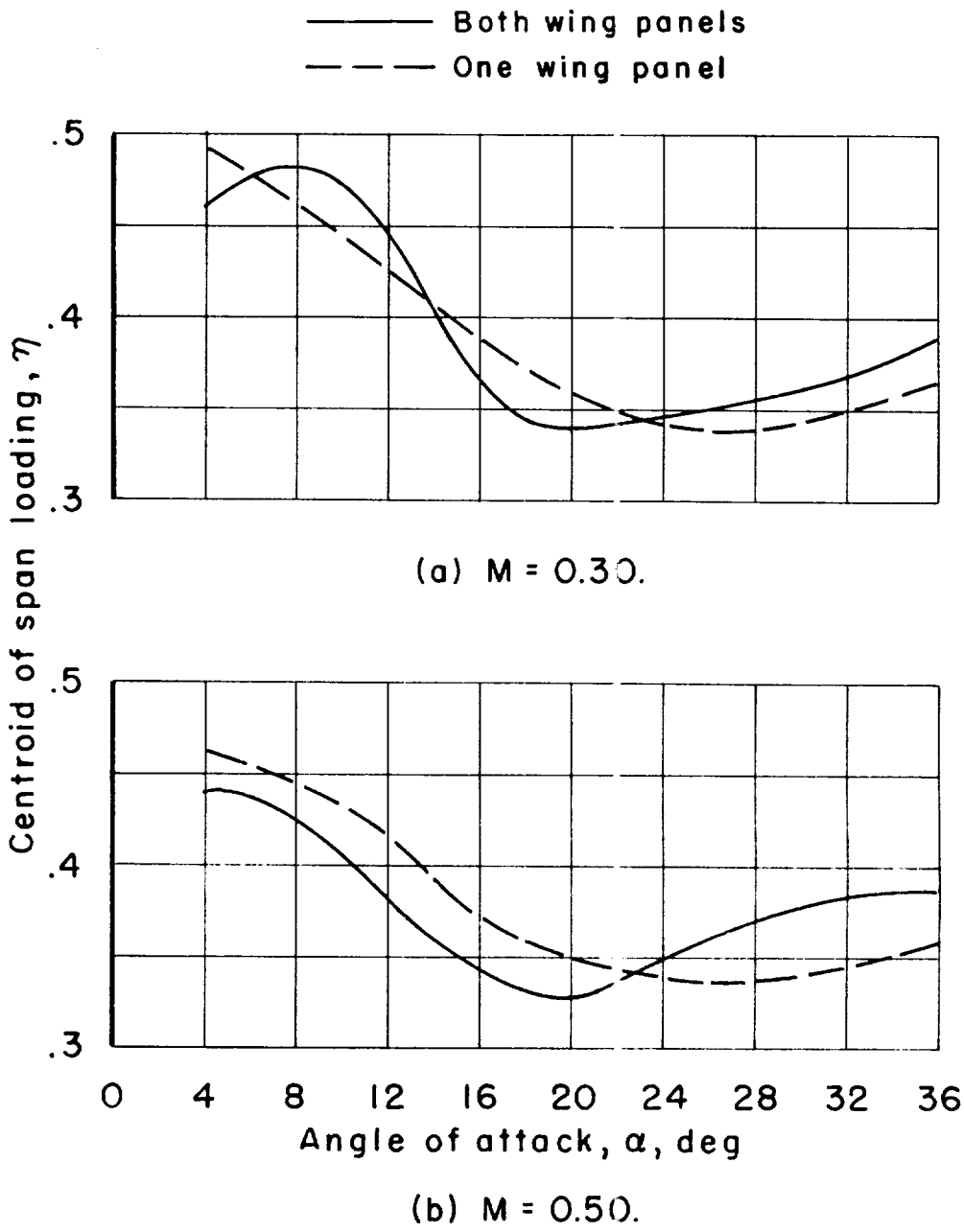

Figure 12.- Spanwise location of centroid of loading.

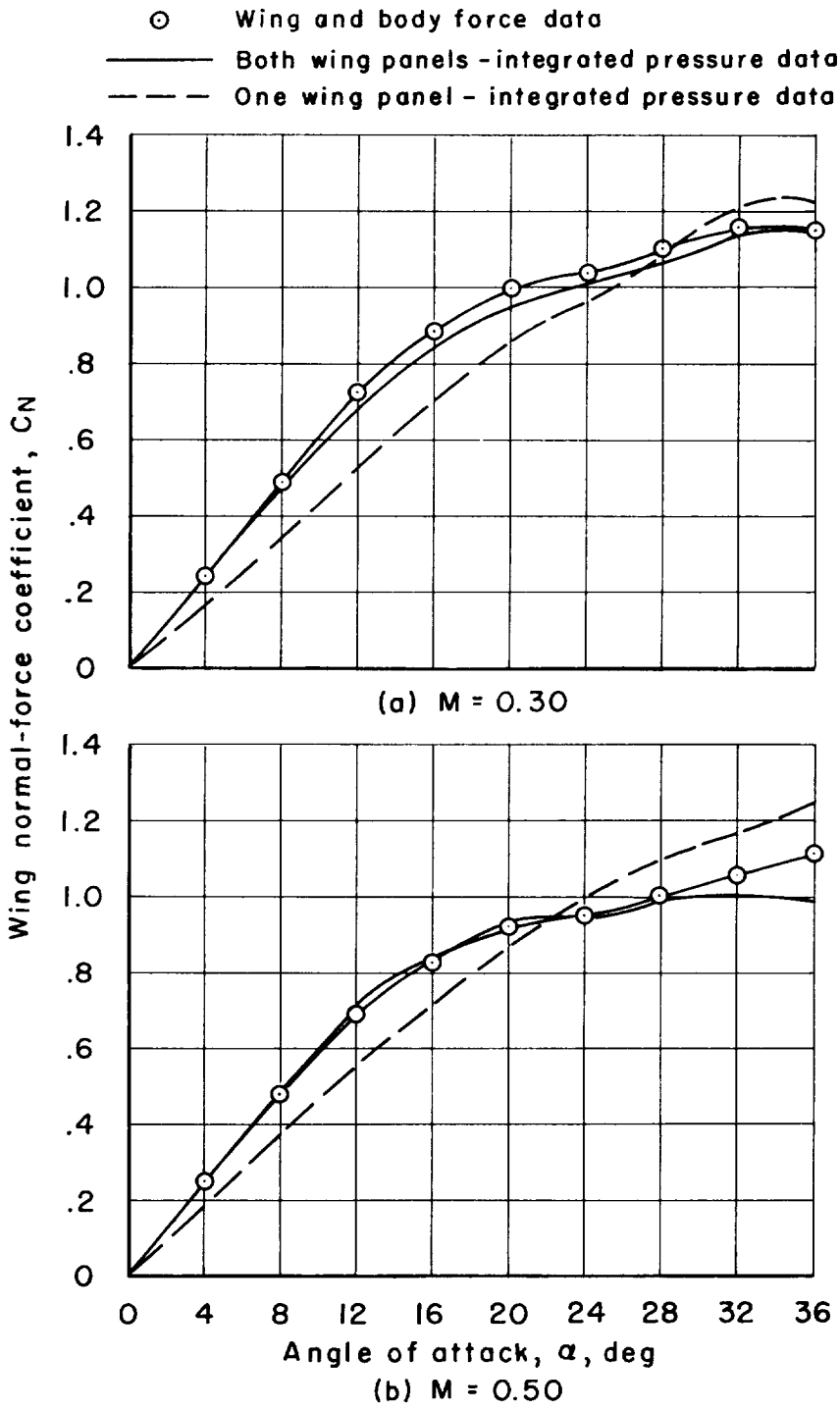

Figure 13.- Comparison of integrated wing normal-force coefficients for the complete wing and for the single panel with wing-body normal-force coefficients from strain-gage balance measurements.

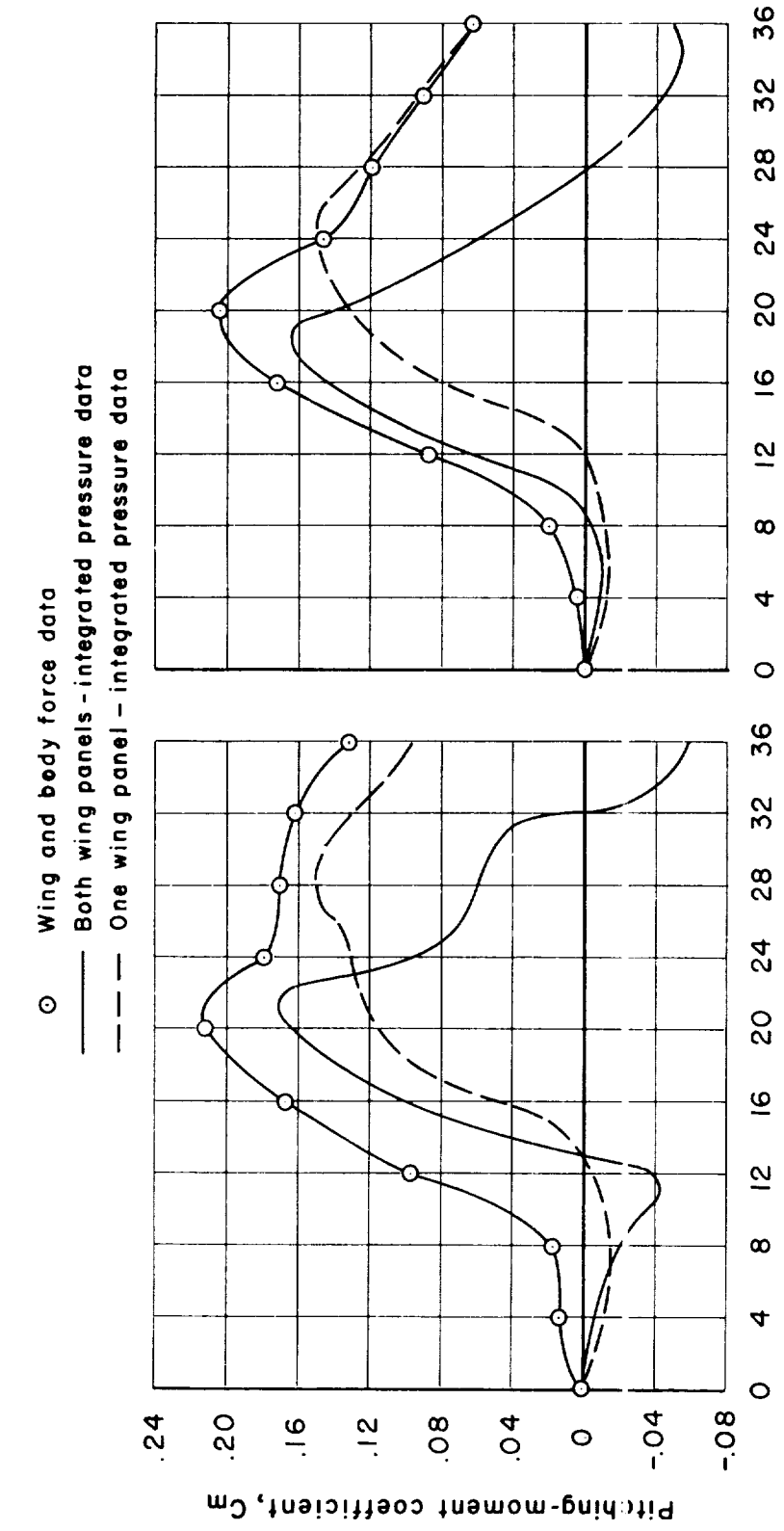

Figure 14.- Integrated wing pitching-moment coefficients and wing-body pitching-moment coefficients from force data.

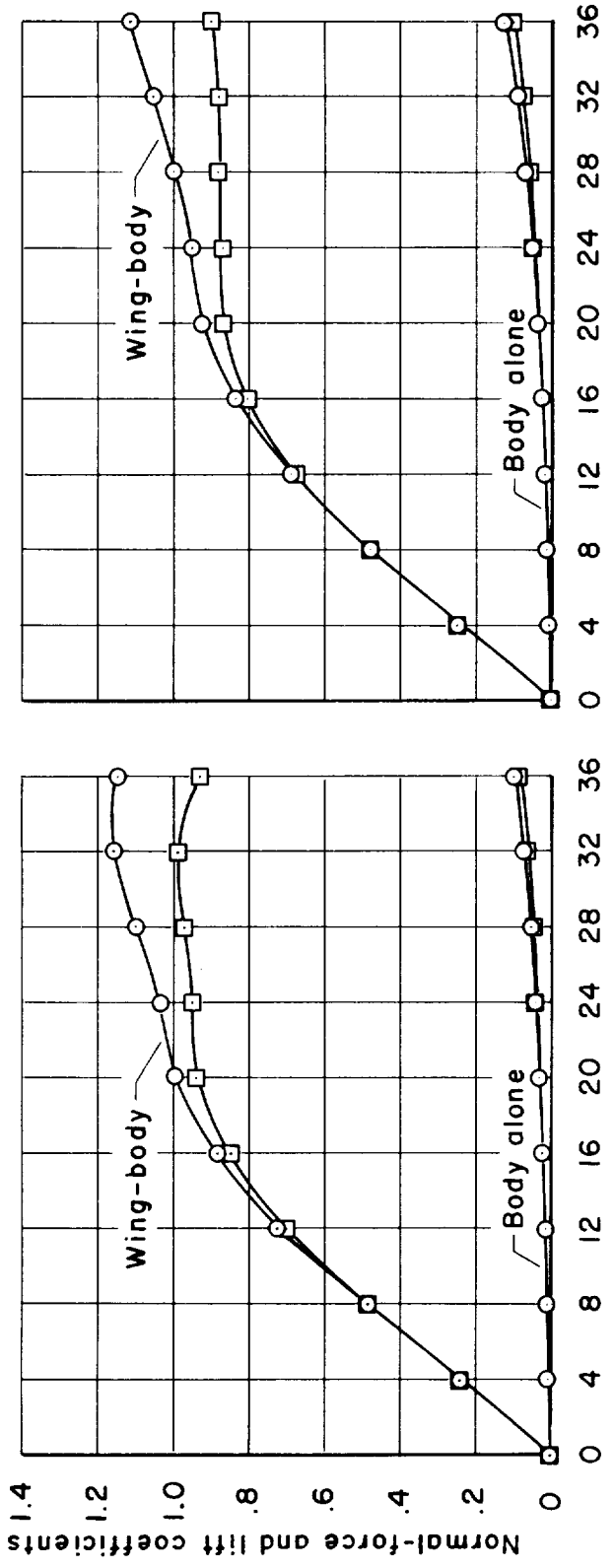

Figure 15.- Lift and normal-force coefficients from force data for the wing and body and for the body alone.

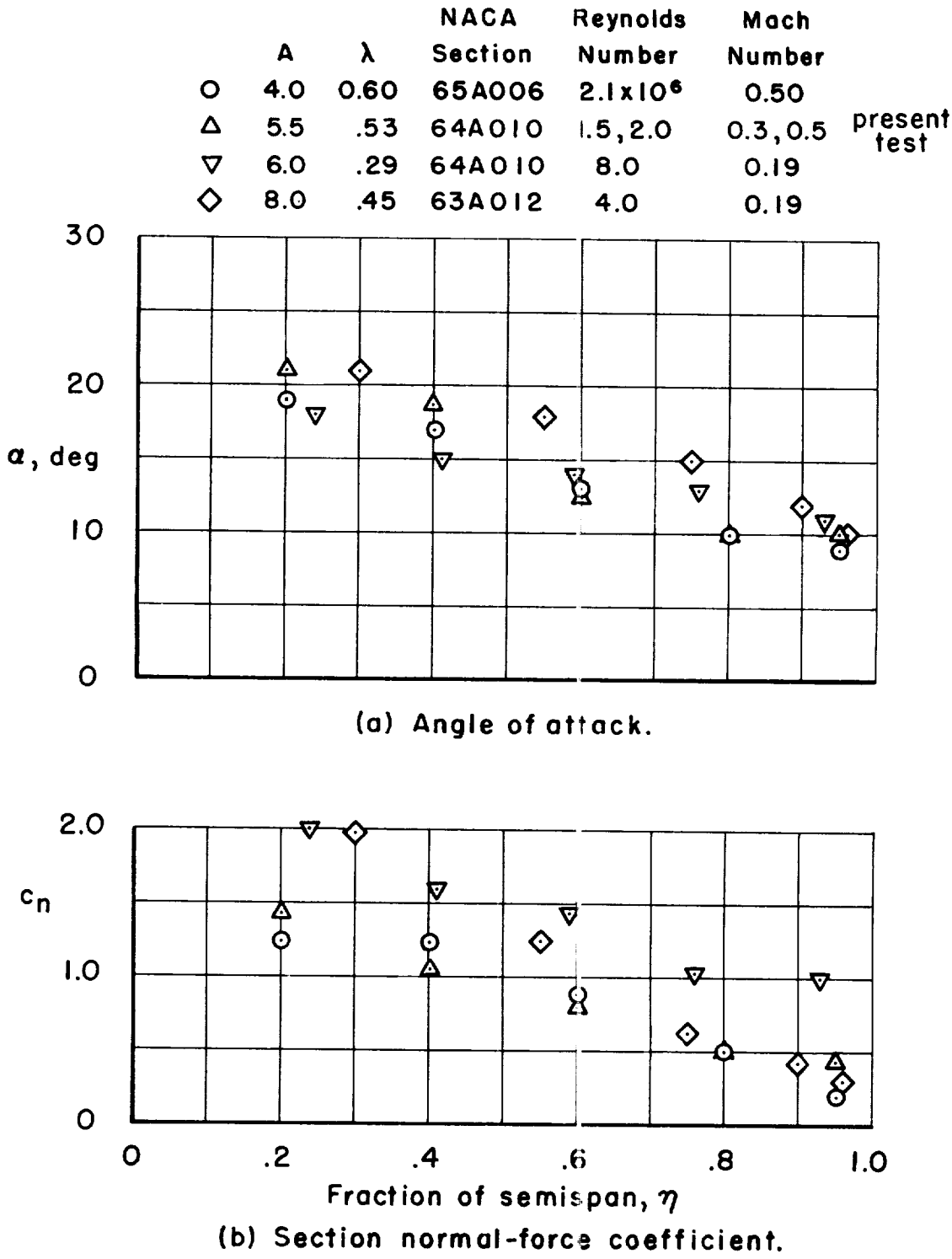

Figure 16.- Correlation of the angles of attack and section normal-force coefficients corresponding to $dc_n/d\alpha \approx 0$ for several 45° sweptback wing and body combinations.

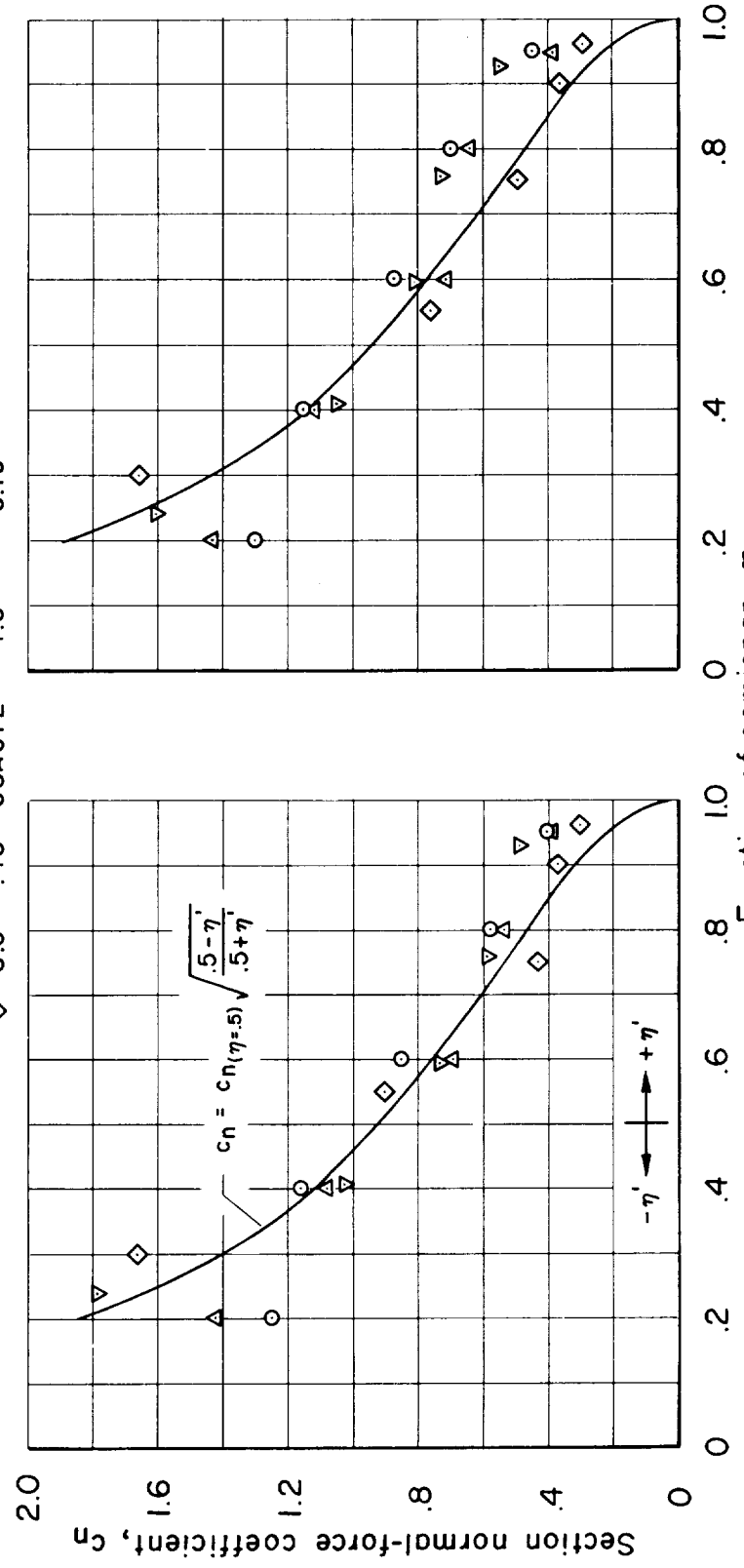

Figure 17.- Summary of section normal-force coefficients for 45° sweptback-wing and body combinations.

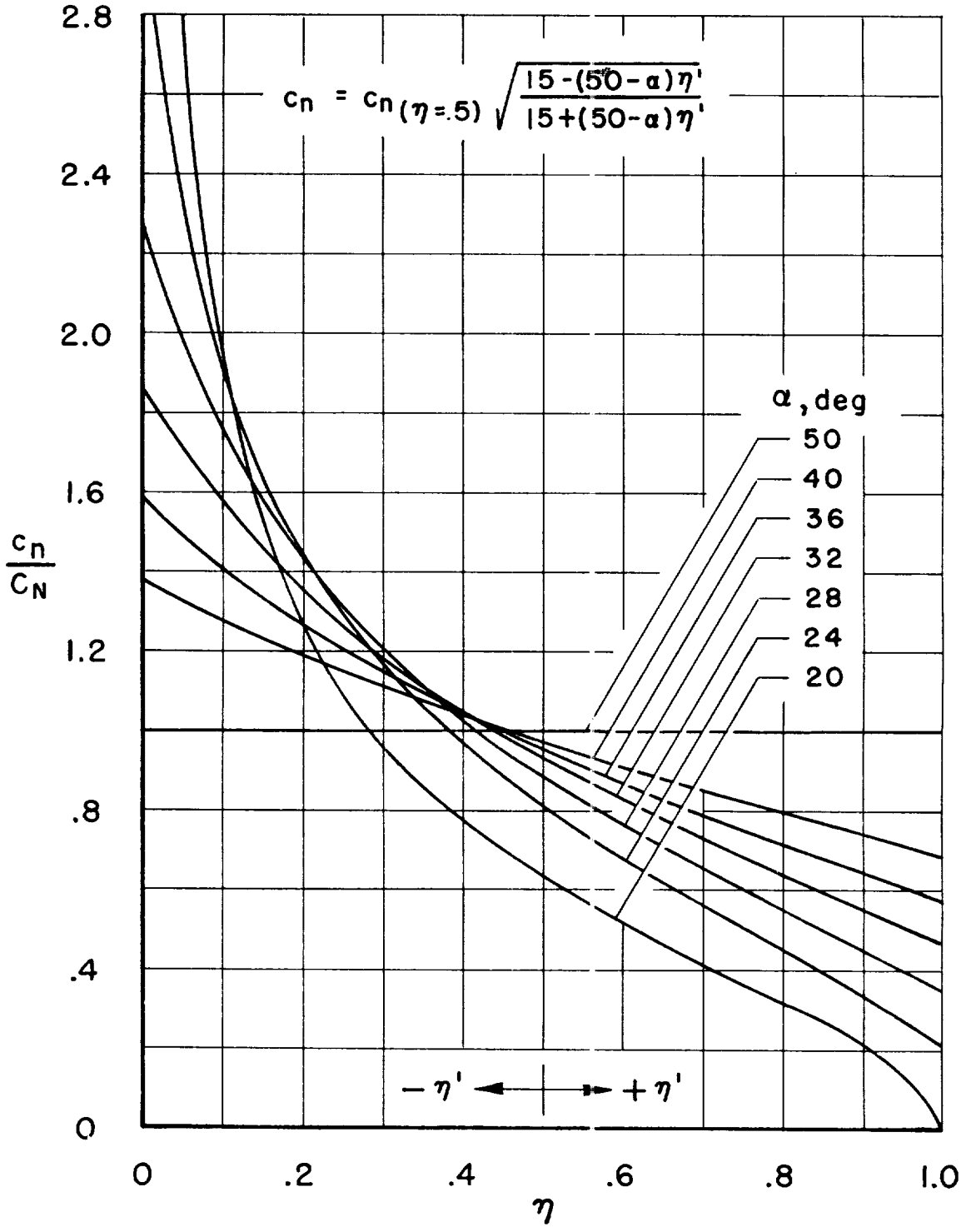

Figure 18.- Derived c_n/C_N distributions for 45° sweptback wings.

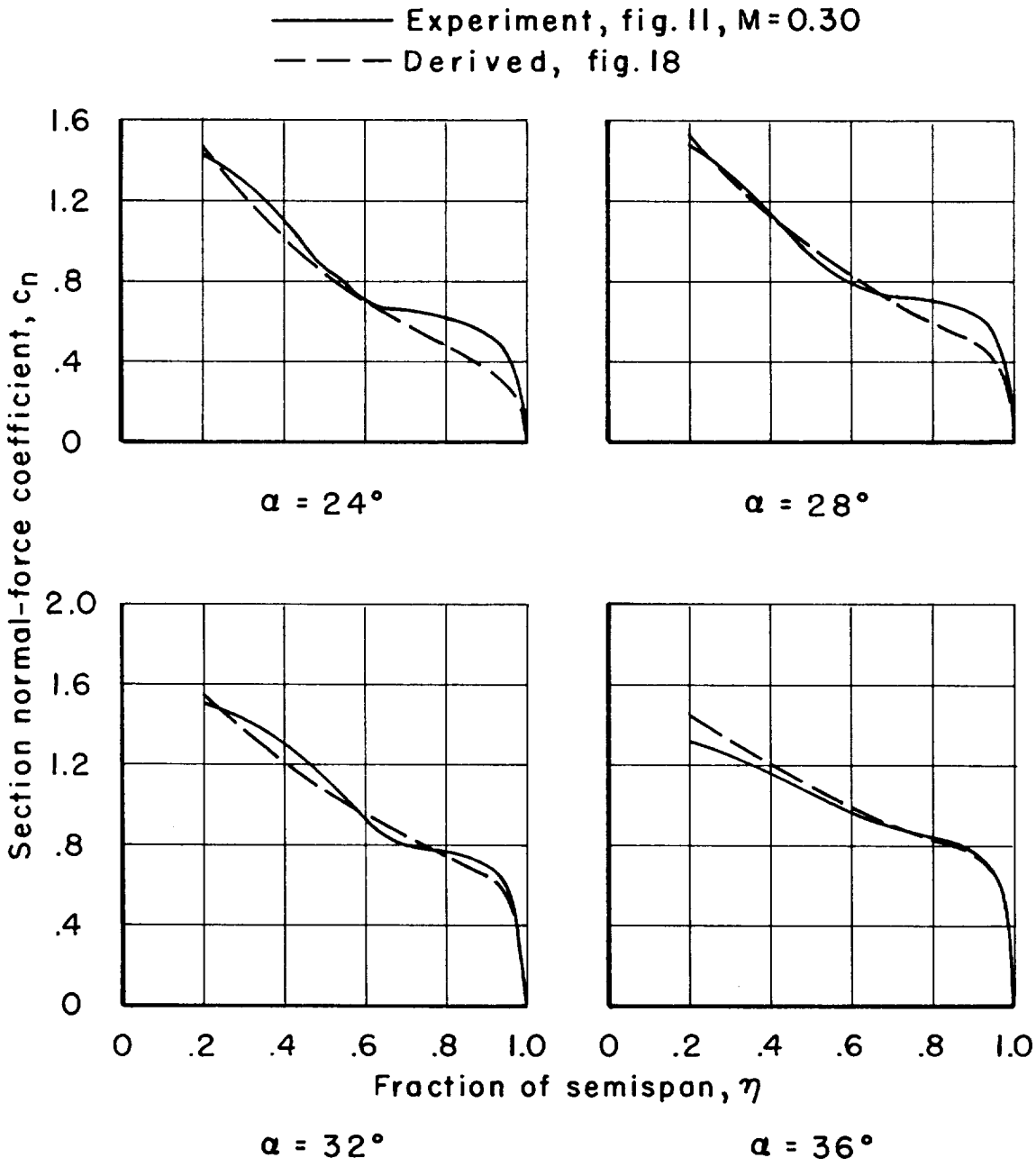

Figure 19.- Experimental and derived distributions of section normal-force coefficient.

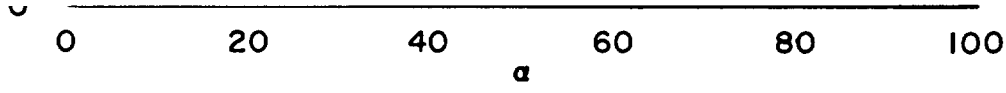

Figure 21.- Velocity ratio and angle-of-attack component for velocity

54

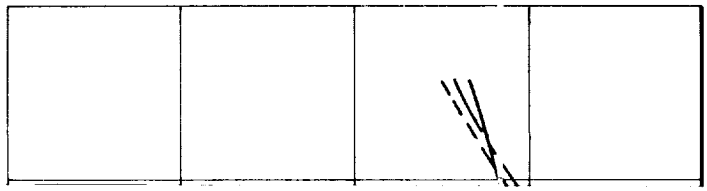

56

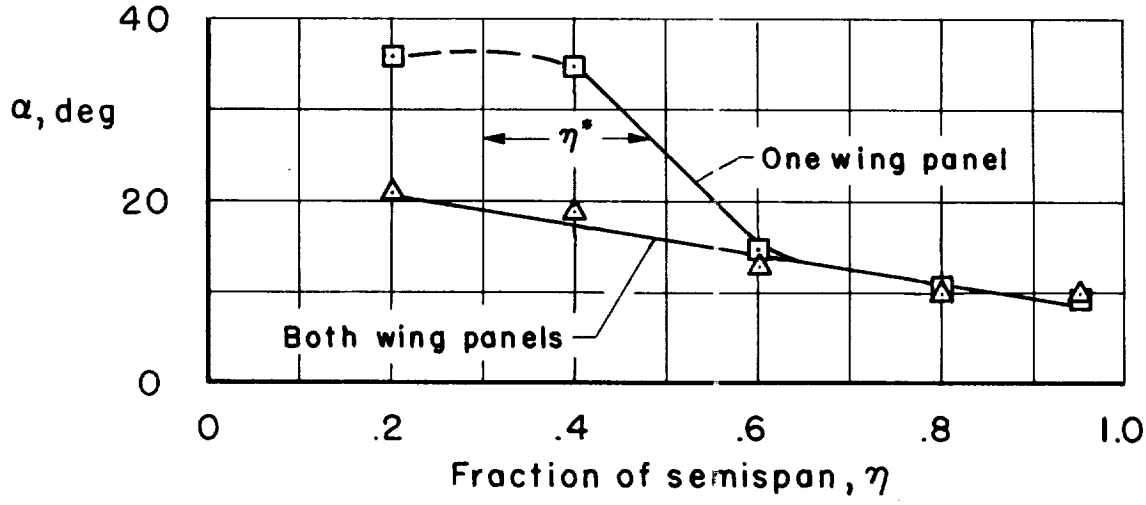

Figure 22.- Angles of attack for $dc_n/d\alpha \approx 0$.

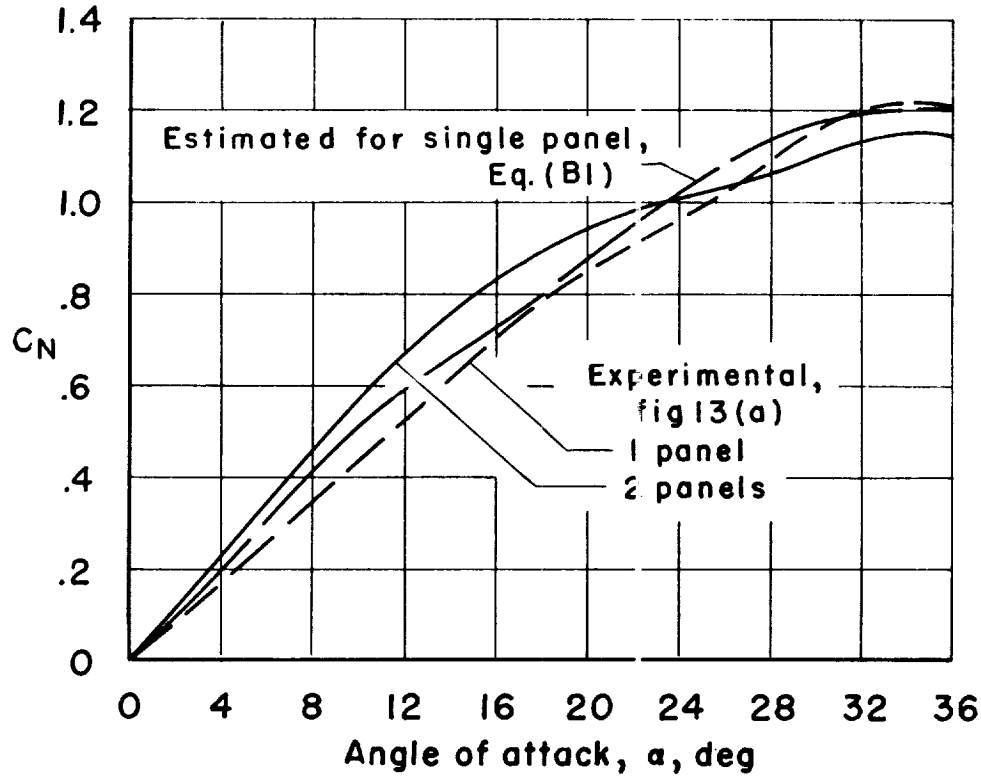

Figure 23.- Experimental and estimated wing normal-force coefficients

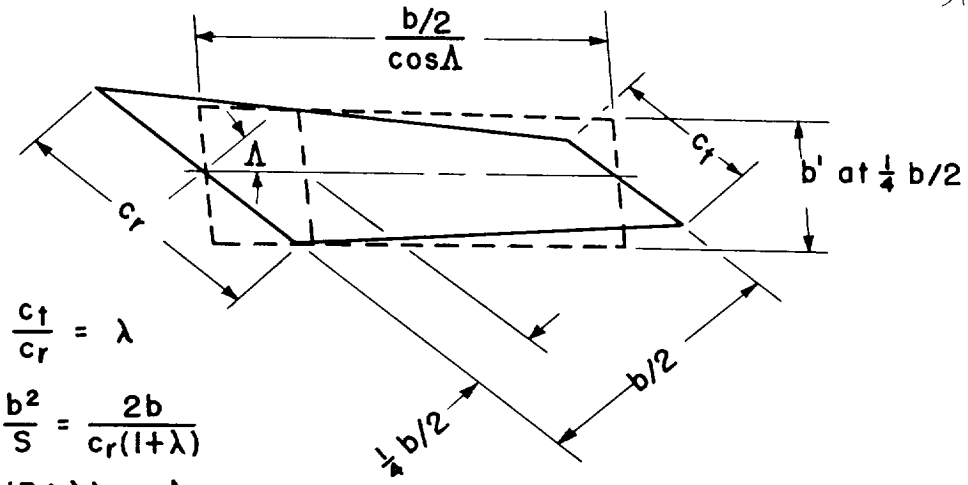

$$\frac{c_t}{c_r} = \lambda$$

$$A = \frac{b^2}{S} = \frac{2b}{c_r(1+\lambda)}$$

$$\frac{b'}{c_r} \approx \frac{(3+\lambda)\cos\Lambda}{4\left\{1-\left[\frac{2(1-\lambda)}{A(1+\lambda)}\sin\Lambda\cos\Lambda\right]^2\right\}}$$

$$A_r = \frac{b'\cos\Lambda}{b/2} = \left(\frac{4\cos\Lambda}{A(1+\lambda)}\right)\frac{b'}{c_r}$$

(a) Swept-wing panel and equivalent wing of low aspect ratio.

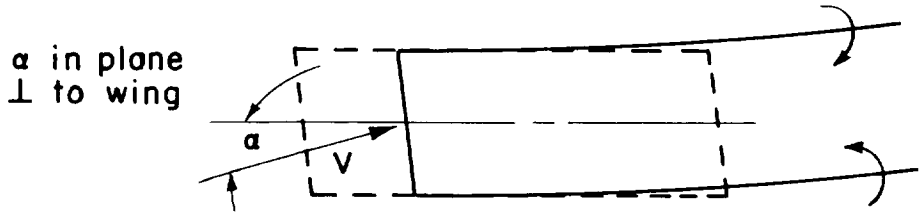

(b) Single-vortex model for low-aspect-ratio wing, unyawed.

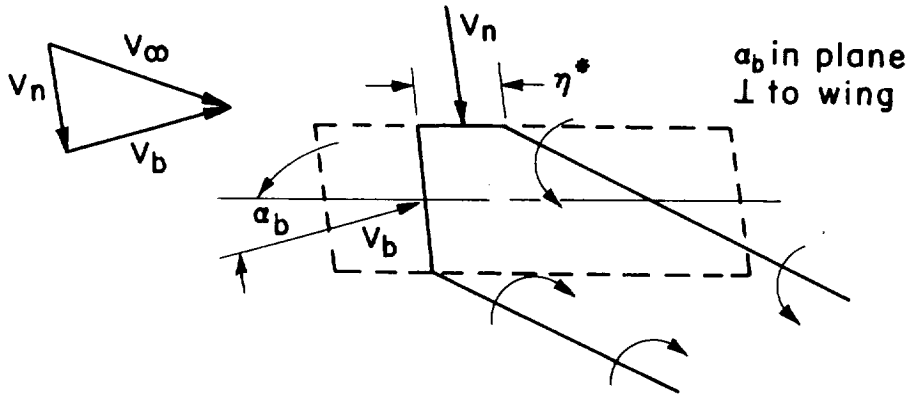

(c) Modified vortex model to account for yaw.

Figure 24.- Conceptual vortex model for the single panel of the swept wing.